

REVIEW ARTICLE

The impact of crystal defects towards oxide semiconductor photoanode for photoelectrochemical water splitting

Qi-Tao Liu¹, De-Yu Liu², Jian-Ming Li³, Yong-Bo Kuang^{2,†}

¹Ningbo Institute of Materials Technology and Engineering, Chinese Academy of Sciences, Ningbo 315201, China

²Nano Science and Technology Institute, University of Science and Technology of China, Suzhou 215123, China

³Petroleum Geology Research and Laboratory Center, Research Institute of Petroleum Exploration & Development (RIPED), PetroChina, Beijing 100083, China

Corresponding author. E-mail: [†]kuangyongbo@nimte.ac.cn

Received March 17, 2019; accepted April 29, 2019

Photoelectrochemical (PEC) water oxidation for sustainable clean energy and fuel production is a potential solution to the demands of organic pollutant removal and growing energy consumption. Development of high performance photoanodes, which is a key component in the system, is one of the central topics in the area. The crystal defect is an old concept but fruiting new understanding with promotive impact to the development of high performance photoanodes. In this review, we elucidated the typical defects involved in the photoanode with the position where they play the roles in the structure and how the properties of photoanode are influenced. In addition, we summarized the feasible protocols to maximize the pros but reduce the cons brought by having defects to the photoanode performance based on recent most prominent research advancements in the field. Finally, we briefly sketched the future perspective with the challenges of this topic when in the scenario of possible developments into practical applications.

Keywords photoanode, defect engineering, oxide semiconductor, water splitting, charge transfer

Contents

1	Introduction	1
2	Substrate-semiconductor interfacial defects	3
3	Defects inside the semiconductor bulk	4
3.1	Contribution to spectral absorption of visible light	4
3.2	Relationship with carrier transportation kinetics	8
3.3	Acting as recombination centers	11
4	Interfacial states between semiconductor and electrolyte solutions	13
4.1	Surface active sites for electrochemical reaction	13
4.2	The Fermi level pinning by surface states	15
4.3	Surface-state passivation	16
5	Outlook	18
	Acknowledgements	19
	References	19

closely linked to our daily life with the accumulated environmental cost paid to industrialization and rocketed energy consumption of modern life. The renewable and ecofriendly energy sources are urgently required to reduce our dependence on traditional fossil fuels [1, 2]. The sunlight, as an abundant clean source, is delivering enormous amount of energy to earth (1.3×10^5 TW) four orders of magnitude more than current global consumption (1.6×10^1 TW in 2010) [3, 4]. Therefore, robust and cost-effective solar conversion is drawing more and more attention from researchers and engineers [5]. Photoelectrochemical (PEC) system offers paths to efficient solar energy harvesting to produce clean hydrogen by solar-driven water splitting, or to yield hydrocarbon fuels by photo-conversion of CO₂ and other low-value organics [6].

High performance semiconductor (SC) photoanode plays a critical role in PEC system and raises the following requirements: (i) rational bandgap deployment for effective light absorption to yield plenty numbers of electron-hole pairs; (ii) suitable band positions which can provide sufficient energy for the activation of electrochemical reactions; (iii) reasonable crystal size that is smaller than the effective carrier diffusion length to facilitate the carrier transportation from the SC interior to the surface; (iv) good long-term stability over hundreds of hours. Unfortunately, in most cases these requirements cannot be

1 Introduction

Environmental issues and energy crises are getting more

*Special Topic: Solar Energy Storage and Applications (Eds. Min Liu and Haotian Wang).

fulfilled easily. For instance, semiconductors (SCs) themselves could be oxidizable at lower anodic potentials than that for water oxidation reaction [7]; furthermore, the sluggish kinetics of the latter one may cause holes to accumulate at the SC-solution interface, and lead to severe charge recombination and further surface corrosion. Besides the surface, the adjustment towards the bulk characteristics of SCs is challenging as well. For example, the real band alignment of the photoanode can be ambiguous due to the uncertain band structure as the result of sensitive relationship between preparation conditions and electronic properties of SCs. Therefore, for improving the properties of photoanode, new methodologies and protocols aiming at crystallinity improvement [5, 8, 9], morphological control [10, 11] and surface modifications [12, 13], etc., are highly desired and attractive to the community. Oxide SCs are among the best candidates considering the material availability, manufacturing cost, and the stability for long-term operation at strong redox potentials [14]. Particularly, regarding the anodic reaction, the oxides are inherently better than other SCs. In addition, there are various preparation routes for oxide materials, with highly tunable properties. Moreover, many other applicable materials in PEC, i.e., nitrides or sulfides, can be conveniently prepared by converting their oxide counterparts. Therefore, we select metal oxides as the major objects in this review, with the discussion slightly extends to other categories.

In recent reports, “crystal defects”, the frequently mentioned concept in solid physics produces numerous new understanding to the PEC electrodes and has been proved as an important variable for tuning their properties and improving their performance. In past decades, defects have been introduced into SCs for modulating their electronic structure, bandgap, conductivity, catalytic performance, etc.. Specifically, since we are focusing on the direct electronic impact of solid-state imperfectness, all “defects” discussed in this review are limited to point defects. However, as a sword of two edges, the defects also act as electron–hole recombination centers which worsen the performance of photoanodes. Therefore, it is necessary to understand the essential role of different defects in scenarios, and the mechanism behind their impact towards specific photoanodes, for the sake of improving the photoanode performance.

For the convenience to describe and discuss the defects in oxide SCs, we would like to briefly introduce the typical classification of them using TiO_2 as an example. Their specific influence in photoanodes is discussed in following paragraphs. In this review, the well-accepted defect notations for nonstoichiometric compounds proposed by Kröger and Vink were used, such as the commonly seen defects of TiO_2 listed below in Table 1.

In this review, we discuss the photoanode performance affected by defect based on the configuration of a typical n-type SC photoanode [see Figs. 1(a, b)]. As shown

in Figs. 1(b, d), the inserted hole blocking layer could suppress effectively R_1 recombination path [see Fig. 1(c)]. Hole transport layer (also called passivation layer) could passivate surface state which increases the electron–hole pair recombination [Fig. 1(c) R_{ss}] and lead to Fermi-level pinning in some extent [compare Fig. 1(c) with Fig. 1(d)]. In addition, the four-electron oxygen evolution reaction requires a large overpotential to complete. To overcome this overpotential, photoanodes are usually coupled with efficient oxygen evolution catalysts [see Figs. 1(b, d)], and

Table 1 Ionic and electronic defects in TiO_2 according to the Kröger–Vink notations [15].

Description	Kröger–Vink notation
Ti^{4+} ion in the titanium lattice site	$\text{Ti}_{\text{Ti}}^{\times}$
Ti^{3+} ion in the titanium lattice site (quasi-free electron)	e'
Titanium vacancy	$\text{V}_{\text{Ti}}^{\prime\prime\prime}$
Ti^{3+} in the interstitial site	$\text{Ti}_i^{\cdot\cdot}$
Ti^{4+} in the interstitial site	$\text{Ti}_i^{\cdot\cdot\cdot}$
O^{2-} ion in the oxygen lattice site	$\text{O}_{\text{O}}^{\times}$
Oxygen vacancy	$\text{V}_{\text{O}}^{\cdot}$
O^- ion in oxygen lattice site (quasi-free hole)	h^{\cdot}

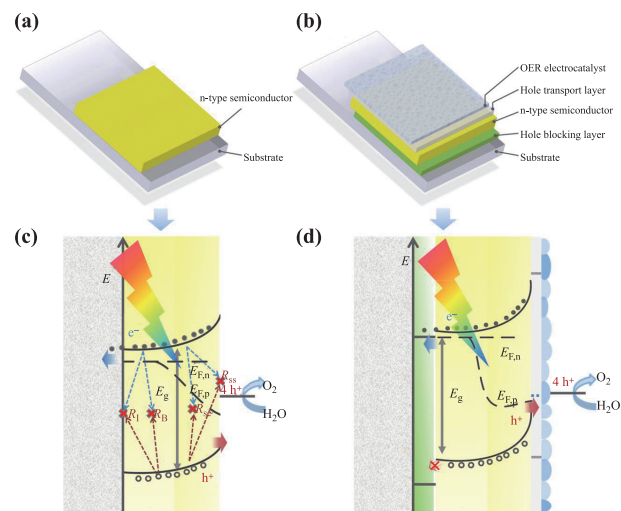


Fig. 1 (a) The schematic structure of a bare photoanode. (b) The schematic structure of a typical photoanode. (c) Quasi-static band diagram with charge transfer and recombination pathways of an extremely simplified photoanode (with only n-type SC) in contact with the electrolyte under continuous illumination corresponding to (a). (d) Quasi-static band diagram and charge transfer of an operating photoanode under continuous illumination in contact with the electrolyte at same bias corresponds to (b). R_1 is the recombination pathway at interfacial defects between substrate and n-type SC; R_B is the bulk defect induced recombination; R_{sc} is the recombination in space charge layer; R_{ss} is the surface-states induced recombination; $E_{F,n}$ and $E_{F,p}$ are the quasi-Fermi levels of electrons and holes under illumination, respectively.

thereafter elucidate the roles of the defects in the sequence of geometric configuration of interfaces or components, which is outlined below [see Fig. 1(c)]: i) interfacial defects between the substrate/current collector and the SC; ii) defects in the n-type SC; iii) defects on SC surface or SC/solution interface.

In later sections, the roles of defects play in PEC reaction and how they affect the properties of photoanodes are discussed individually following the order above. To take one step further, we summarize the feasible or possible routes based on most prominent research advancements in these fields by using defect engineering as the key method for improving photoanodic performance.

2 Substrate-semiconductor interfacial defects

The importance of this interface has been long recognized by researchers from the area of electric engineering due to its essential role for realizing high-performance metal-oxide-SC field-effect transistor and other electronic devices [16, 17]. But unfortunately, the PEC community has only started to realize its critical role from recent years. Even though, right after more attention was given to the structural defects in this region and the junction against the back contact [18–23]. Liang *et al.* [24] suggested that the presence of defect states in fluorine-doped tin oxide (FTO) substrate acting as recombination centers undermining photoelectronic properties of the photoelectrodes, As can be seen in Fig. 2(a), and with the photogenerated electrons being trapped in defect sites, negative charges accumulate at the SC/FTO interface, preventing the electron transport from SC to FTO. In addition, Souza *et al.* [19] suggested that stress induced by the strong interaction between the hematite and the FTO substrate can cause the formation of defects on hematite surface that increase the recombination of electron–hole pairs. The lattice distortion can generate electron band distortion in some extent, thus, intermediate defect levels formed close to the conduction band serve as recombination centers decreasing the properties of hematite. These phenomena have been commonly reported in the cases of hematite and BiVO₄ photoanode [18, 20, 21, 25]. Therefore, the defects in this junction [see Fig. 2(a)] act as recombination centers that quench the electron–hole pairs and degrade the PEC performance drastically. In order to reduce the issue raised by these counteractive defects, several rational and effective paths were applied in recent reports, such as by inserting a thin metal-oxide layer between substrate and SC as the hole blocking layer [18, 21, 26–28] [see Fig. 2(b)] or host scaffold-guest absorber structures [29–31]. These means were also used extensively in solar cells for similar reason [32, 33].

The hole blocking layer has been reported widely. In general, they have some common features or material requirements. For instance, such interlayer metal oxides have relatively large band gaps and valence band (VB)

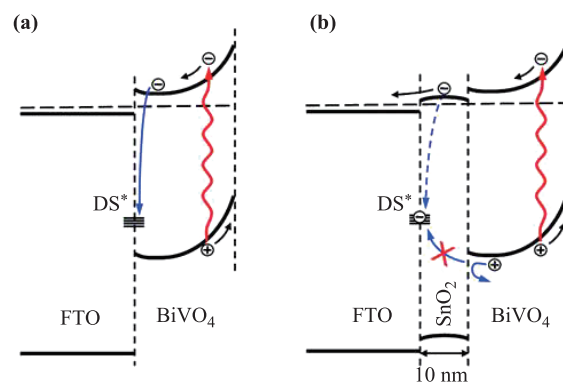


Fig. 2 The schematic diagrams (a, b) illustrate the recombination at the defect state present at the FTO/BiVO₄ interface and the hole mirror effect of the SnO₂ layer, respectively. Reproduced from Ref. [24], Copyright © 2011 American Chemical Society.

edges deeper than that of the light absorbing SC layer. The resulting tandem configuration prevents the hole recombination in defect sites with electrons from the conduction band (CB) by rectifies the carrier flow [see Fig. 2(b)]. In some cases, the inserted interlayer decreases the stress between SC and substrate and imperfect crystal alignment, the defect content is reduced greatly, thus decreasing the electron–hole recombination at the interface. For instance, by introducing SnO₂ [24, 25, 27, 34] layer to replace the initial interface, as shown in Fig. 2(b), can realize this concept. Byun *et al.* [25] have investigated the thickness effect of the SnO₂ buffer layer on the properties of BiVO₄ based photoanode. Interestingly, the structure of BiVO₄ answers to the thickness changes of SnO₂ buffer layer, with effects of crystalline phases and grain size. The photocurrent increased with smaller grain size and smoother surface of BiVO₄ as the SnO₂ thickened from 0 to 65 nm.

In addition, Hisatomi *et al.* [35] reported the deposition of beneficial Ga₂O₃ underlayer for hematite by atomic layer deposition, for reducing its lattice mismatch with the substrate. The nucleation and growth mode of hematite films were modulated by the Ga₂O₃ underlayer. The greatly improved crystallinity and uniformity of hematite films thus notably improved the photocurrents of electrodes. However, a certain thinness of Ga₂O₃ underlayer was required due to the poor crystallinity of very thin films.

Regarding the significance of the quality of hole blocking layer, i.e., crystallinity and pin-hole-free requirement, great efforts have been dedicated to the selection and realization of new coating materials. For instance, beyond SnO₂, Hisatomi *et al.* [29] reported a 9 nm Nb₂O₅ layer can effectively prevent the recombination between photoexcited holes and electrons at the FTO-Fe₂O₃ interface. In the meantime, it is also helpful to suppress electron–hole recombination in hematite bulk by its rectifying contact with Nb₂O₅ layer. The interlayer can be even thinner. Zhang *et al.* [18] reported that an ultrathin lutetium ox-

ide (Lu_2O_3) film could be deposited as the hole blocking layer by pulsed laser deposition. Besides a deeper VB edge than that of BiVO_4 , which is the minimal requirement for the hole blocking layer, the peculiarity of using Lu_2O_3 is the lattice matching. The deposited 1.4 nm Lu_2O_3 layer could notably increase the photocurrent density and improve the carrier separation efficiency, suggesting that the presence of Lu_2O_3 layer matched FTO and BiVO_4 lattices and helped minimizing the number of structural defective recombination centers formation at these interfaces. Similar to oxides, lately using the GaN as the hole blocking layer for Ta_3N_5 photoanode also gave a 1.8-fold enhancement to the efficiency, due to effective depression of the recombination pathway by the high quality GaN [26]. Therefore, as we mentioned above, carefully selected hole blocking layer with high crystallinity and minimized number of defects is highly desired for improving the PEC performance.

Beyond planar layer by layer structures, similar band layout can be used in more complicated hierarchical nanostructures. Host scaffold-guest absorber structure have been reported widely [29–31, 36], in which the light absorbing nanosized guest material was attached to a nanostructured host scaffold. Similar to the above hole block layer in the photoanode assembly, oxides such as WO_3 [31, 36], SnO_2 [37], and Nb_2O_5 [29], were used as the scaffolds because of similar band requirements of Valence Band Maximum (VBM). Since their motif on the design of interface is very similar to hole blocking layers and the designing challenge relies more on the morphological issue, discussions on them are not included.

In short, the substrate-SC interfacial defects are a critical issue for maximizing the potential of high performance photoanodes. Such a layer has been proved to require high crystallinity and precise thickness control that could be achieved by reliable coating technique. Furthermore, matching between lattices of both sides are highly desired, although in most cases such a demand is hard to be fulfilled. Nonetheless, even though the inserted hole blocking layer could enhance the PEC properties in some extent, the cognition of specific interface defect formation still remains ambiguous. Therefore, it is essential to figure out the concrete form of this defective interface for further improving the PEC performance in the future.

3 Defects inside the semiconductor bulk

Defects in the bulk of SC are mainly the result of crystallinity issues or doping. The intrinsic imperfectness or heteroatom in SC crystal structure strongly disturbed the periodic arrangements of perfect crystals and greatly changed the electronic behavior of the material. Such a statement is true not only for simple SC like single crystal silicon, but also for oxides although their structures are way more complicated. Regarding the importance of de-

fects, tremendous amount of efforts have been made both experimentally and theoretically for elucidating their roles in various oxide SCs. To date, diverse defects were studied and even their role was well illustrated in several binary oxide systems. But for ternary or more complicated compounds, to understand a particular type of defect among many of them could be extremely challenging. Thus, in here we will focus on their overall impact to the physical properties of SCs rather than the mechanistic details. Considering the defects have both advantageous and adverse impact to the material, we would like to discuss their roles from following aspects: i) contribution to spectral absorption of visible light; ii) relationship with carrier transportation kinetics; iii) acting as recombination centers.

3.1 Contribution to spectral absorption of visible light

The spectral absorption range of SCs is of manifest significance for the PEC systems. Since the absorption is directly linked to the band structure of the SCs, the terms of “wide bandgap” and “narrow bandgap” are frequently used regarding this topic. However, the “narrow” or “wide” is not precisely defined to a certain number, but rather related to the context of the SCs application. In PEC and photocatalysis community, the divide was usually implied to about 2.4 eV, which corresponds to the spectral maximum of the solar energy, or around 3.0 eV as the edge of visible light. For instance, many oxides of highest oxidation state with empty valence d-orbitals, such as TiO_2 , Nb_2O_5 , V_2O_5 , and Ta_2O_5 , are wide bandgap SCs. They cannot absorb an ample portion of solar light, resulting in poor overall solar to chemical conversion efficiencies. Using a simple integration of the solar spectrum, the theoretical conversion limit can be estimated [assuming a 100% incident photon-to-current efficiency (IPCE) of the photoelectrode]. Given the visible light carries more than 40% of solar energy rather than ~2% of UV light, the necessity is evident to utilize both. Therefore, effective approaches for modulating the electronic structure of metal oxides are urgently needed to extend their spectral absorption range.

Herein we use TiO_2 , a classical wide bandgap SC, as an example to elucidate the route of employing doping and defects to reduce bandgap for enhancing visible light harvesting. TiO_2 was used for PEC water oxidation in the earliest report [38]. Since the wide bandgap (3.2 eV) limits its light harvesting to UV range, its photocurrent and overall efficiency was predominately restrained. On the other hand, the great stability, unobstructed internal charge transportation and low cost made TiO_2 still as an attractive candidate for practical PEC systems. Various developments have been made by sensitizing or fabricating hybrid structures. However, the material itself still can be further engineered to reach out a better absorption, and one of the most feasible strategy is defects introduction. With this concept, numbers of preparation and perfor-

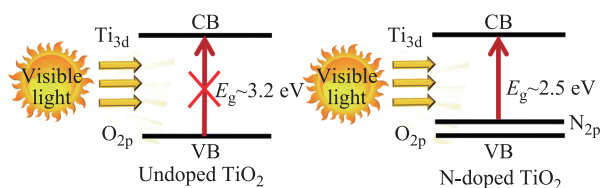


Fig. 3 Energy level diagrams for undoped and N-doped TiO_2 . Reproduced from Ref. [55], Copyright © 2016 Royal Society of Chemistry.

mance study on defective titania, i.e., yellowish TiO_2 [39], black TiO_2 [40–42], red TiO_2 [43] have been reported in recent years.

It is straightforward that the color of TiO_2 is related to its band gap width. The yellowish TiO_2 is the result of the absorption edge being slightly extended from UV to visible and the bandgap being decreased from ~ 3.2 eV to about 2.3–2.8 eV [39, 44–46]. Doping with nonmetal elements, such as N [46–50], S [39], P [51], and F [52, 53] can produce TiO_2 with large quantity of defects and the yellowish appearance. The basic concept is similar to using Bi^{3+} , Sn^{2+} or Pb^{2+} , that introduces new orbitals to

mix with O_{2p} components of the VB [44, 54, 55], resulting in the valance band shift to negative direction due to the mixture of N_{2p} and O_{2p} states, as shown in Fig. 3. The difference is the quantum selection rule leads to different absorption coefficient corresponds to s-d and p-d transitions. Various elements can serve as dopant for TiO_2 , however, N was the most popular one among them [41, 47]. For example, Wang *et al.* [46] reported that the N-doped TiO_2 bowl nanoarrays with decent visible response. The higher N-doped contents in TiO_2 bowl nanoarrays corresponds to larger photocurrent which agrees with the narrowed bandgap of $\text{TiO}_2\text{-NH}_3$ is 2.7 eV, whereas $\text{TiO}_2\text{-N}_2$ bandgap is 3.0 eV, similar to regular TiO_2 .

Furthermore, the position of doped N atoms can be controlled by the experimental conditions. For instance, N-doped TiO_2 nanowire arrays was prepared by N-implantation (notation N- TiO_2) and its subsequently annealed sample was applied to PEC water splitting [48]. The N implantation changed the color of TiO_2 NW arrays from white to green, indicating the occurrence of N-doping, and further to brilliant yellow after annealing, as depicted in Fig. 4(a), corresponding to the removal of interstitial-N atoms and the evolution of substitutional-

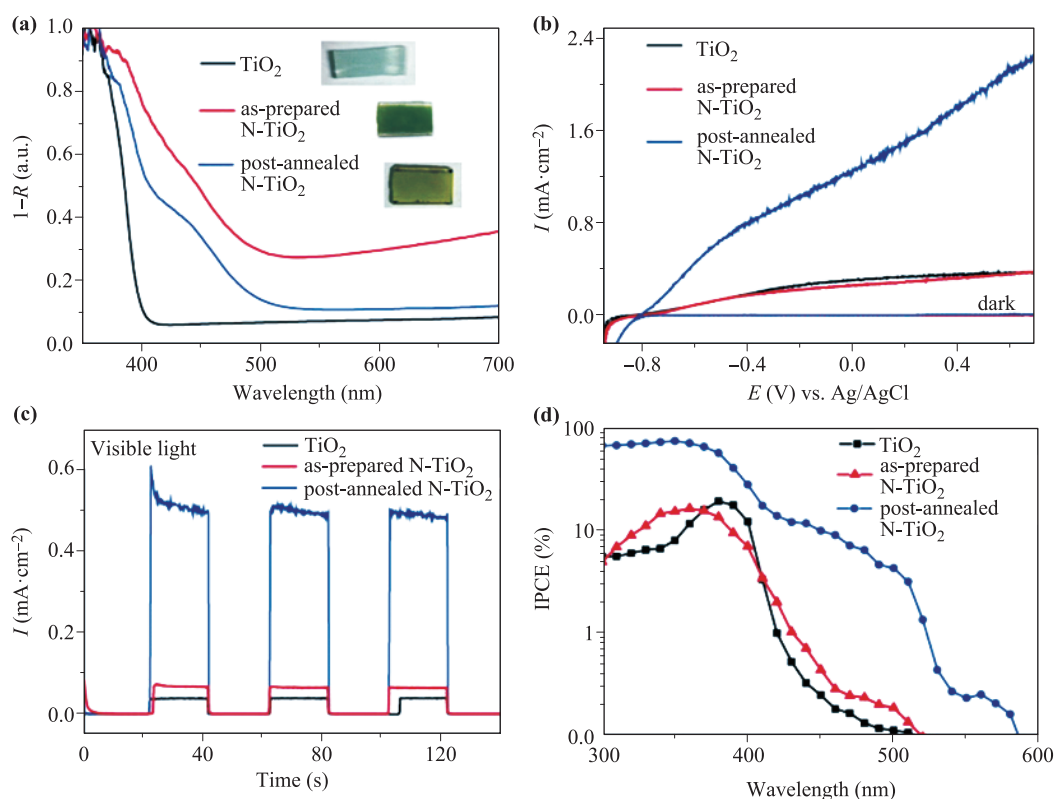


Fig. 4 Characterization and PEC performance of TiO_2 and N- TiO_2 NWs. (a) Light absorption properties of TiO_2 , as prepared N- TiO_2 , and post-annealed N- TiO_2 . The insets are the digital photograph of these samples. (b) Linear sweep voltammograms of pristine TiO_2 , as prepared N- TiO_2 and post-annealed N- TiO_2 under 100 mW/cm^2 xenon light illumination with a scan rate of 20 mV/s in 1.0 M NaOH aqueous electrolyte. (c) Photoresponse of TiO_2 , as-prepared N- TiO_2 and post-annealed N- TiO_2 NWs under chopped visible light illumination ($>400 \text{ nm}$) at $0.5 \text{ V vs. Ag/AgCl}$. (d) IPCE spectra of TiO_2 , as-prepared N- TiO_2 and post-annealed N- TiO_2 NWs collected at $0.5 \text{ V vs. Ag/AgCl}$. Reproduced from Ref. [48], Copyright © 2015 American Chemical Society.

N atoms via N atoms being captured by V_{O} . This final structure showed absorption edge extended to 530 nm. The photocurrent and IPCE for visible light absorption was enlarged by an order of magnitude, proving the importance of N-atoms in specific sites [see Figs. 4(b–d)].

Besides of considering only one type of sites, different defects can occur simultaneously. For instance, Premkumar [54] proposed that V_{O} could be generated accompany with the nitrogen doping. The band gap of $\text{TiO}_{2-x}\text{N}_x$ was further narrowed by shifting up VBM by N_{2p} and lowering CBM due to the presence of V_{O} , decreasing the bandgap from 3.2 eV to 2.8 eV. However, the physical mechanism of V_{O} for reducing the bandgap was illustrated by reports [54, 56]. Specifically, V_{O} results in local states below the CB edge. The V_{O} local state can accept electrons from the VB by visible light excitation. Therefore, V_{O} are called Frenkel centers (F_{ch} centers) [56]. Besides, the electron trapped in V_{O} could interact with Ti^{4+} and reduce it to Ti^{3+} species, whereas the Ti^{3+} defect contribute to visible range response as well, due to its serving as shallow donors below the CB. Recently the co-doping route for reducing the bandgap of TiO_2 was widely used given its more flexibility of controlling the band structure, which leads to the development of several high performance photoanode [57, 58].

Heavy doping to TiO_2 with suitable energy state may even half the bandgap width. Such a condition produces black TiO_2 and was reported firstly by Chen *et al.* [41]. It can enhance solar absorption of regular white nanophase TiO_2 by introducing a disorder surface layer, namely black TiO_2 , through hydrogenation. It presents a striking contrast to TiO_2 primitively both in color and in the light absorption. The tremendous amount of reduced Ti species almost completely removed the lattice structure near the surface of SC, and yields mid gap states whose energy distribution differs from that of a single defect in crys-

tal. Therefore, a band tail states was formed by continuum extending of mid-gap states, thereby overlapping with the CB or VB edge instead of forming discrete donor states [see Fig. 5(b)]. In addition, the disordered surface layer can provide enough trapping sites for photogenerated carriers and prevent them from rapid recombination, which is quite different with other SCs discussed in later paragraphs. As depicted in Fig. 5, the light absorption properties were enhanced by reducing the bandgap width from 3.2 eV to 1.54 eV. Other strong reducing conditions could produce black TiO_2 as well. For instance, the black TiO_2 can be obtained by melted Al reduction [49, 59]. Moreover, beyond only a surface layer, the black disorder part of above mentioned materials can be solely prepared. According to the report by Liang *et al.* [60], a pure amorphous hydrogen-doped TiO_2 (a- $\text{TiO}_2\text{:H}$) film was prepared using a magnetron sputtering technique under reactive hydrogen plasma. Since the method maximizes the portion of defective part, the structure can gain a similar absorption with much less material and thinner film, which is favorable for carrier transportation. Further combining the black TiO_2 with nanotube arrays (B-TNTs) is another promising approach, such a structure was used in photoanode for water splitting by Cui *et al.* [59]. As depicted in Fig. 6, the light absorption was enhanced drastically, so that the photoanode gave a photocurrent density of 3.5 mA/cm^2 and high ABPE of 1.2%, which is 5 times better than that of the pristine TiO_2 nanotube arrays (TNTs) (see Fig. 6).

Given the large overpotential for OER, a band gap of 1.5 eV like black TiO_2 can be somewhat too narrow for holes to have enough energy. A middle width around 2 eV could be a balanced choice between the light absorption and the energetics of individual carriers. Red TiO_2 materials are suitable for bridging this gap, for instance, the case reported by Yang *et al.* [43], the red TiO_2 display

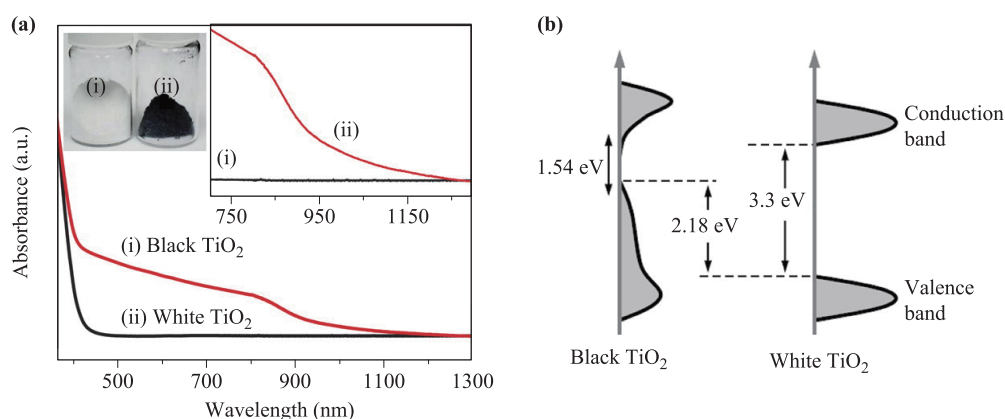


Fig. 5 (a) Spectral absorbance of the white and black TiO_2 nanocrystals. The inset enlarges the absorption spectrum in the range from approximately 750 to 1200 nm. The inset sample photographs comparing between unmodified white and disorder-engineered black TiO_2 nanocrystals. (b) Schematic illustration of the DOS of disorder-engineered black TiO_2 nanocrystals, as compared to that of unmodified TiO_2 nanocrystals. Reproduced from Ref. [41], Copyright © 2011 American Association for the Advancement of Science.

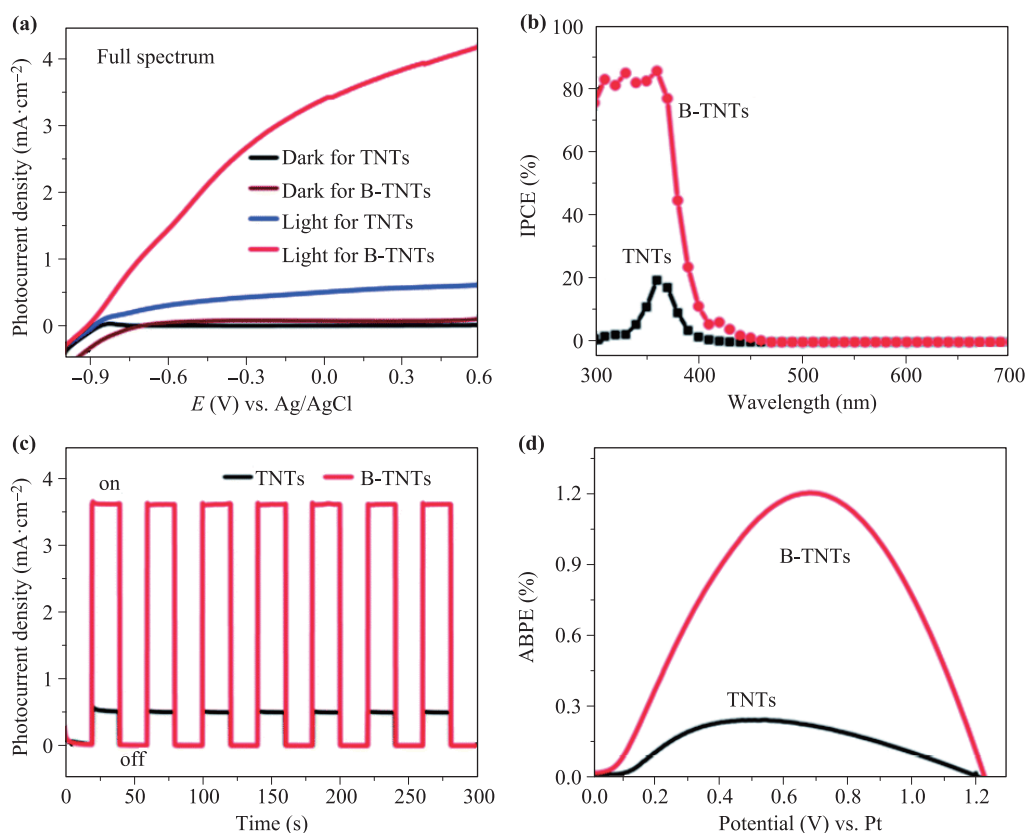


Fig. 6 (a) Linear sweep voltamograms collected under $100 \text{ mW}\cdot\text{cm}^{-2}$ illumination using a three electrodes setup (working TNTs or BTNTs, Pt counter, Ag/AgCl reference electrode, scan rate of $50 \text{ mV}\cdot\text{s}^{-1}$) in 1 M NaOH electrolyte ($\text{pH} = 13.6$). (b) IPCE spectra in the region of 300–700 nm at 0.23 V vs. Ag/AgCl. (c) Transient photocurrent responses of the TNTs and B-TNTs at 0.23 V vs. Ag/AgCl. (d) ABPE of the TNTs and B-TNTs as a function of applied potential. Reproduced from Ref. [59], Copyright © 2014 Royal Society of Chemistry.

the maximum absorption edge beyond 700 nm but the bandgap is larger than black TiO_2 . However, although it is also produced from strong reducing conditions, the chromophore forming mechanism is different from black TiO_2 . ^1H nuclear magnetic resonance (NMR) spectra indicates the presence of new chemical environment of hydrogen species in the red TiO_2 . Moreover, both electron spin resonance (ESR) and extended X-ray absorption fine structure (EXAFS) spectra proved that the hydrogen was introduced into $\text{V}\ddot{\text{O}}$. Combining experimental characterizations with theoretical calculations reveals the excitation of a new sub-valence band associated with atomic hydrogen filled $\text{V}\ddot{\text{O}}$. It is different with the discrete band yield by $\text{V}\ddot{\text{O}}$ below the edge of CB for trapping photogenerated electron [56], even though the bandgap width decreased in both structures.

We have discussed the pivot role of defects for modulating the bandgap width via introducing new electronic states to TiO_2 . The concept here offers an angle of view about the manipulation of defects for narrowing band gap, although the great chemical diversity between different oxide materials may make it not likely to use the experience

of TiO_2 to other systems directly. The motif is applicable to other oxides, for instance, ZnO , Nb_2O_5 , and S-doped BiVO_4 and N-doped BiVO_4 with various doping and thermal processing protocols [61–65]. However, the occurrence of various defects with a raveled impact is quite common, particularly for ternary oxides or mixed valence state oxide. Such a situation can be very challenging for solving out the physical mechanism which precisely reflects the energy band change, but on the other hand, the engineering based on PEC performance is still workable. By combining the evaluation of external quantum efficiency (EQE), IPCE and the absorption spectrum, the contribution from enhanced absorption can be extracted in most cases.

An extreme situation of doping, in which an overwhelming amount of dopant level was introduced, could completely restructure the crystal into new phases. The ternary metal oxide, such as BiVO_4 [10, 66], SnNb_2O_6 [67, 68], and PbMoO_4 [69], was formed by introducing Bi^{3+} , Sn^{2+} or Pb^{2+} to metal oxide for narrowing the SC bandgap to the range of visible light [70]. The concept is that, the initial VB of the binary oxides counterparts, which mainly consists O_{2p} orbitals, was hybridized with

the orbitals of Bi 6s in Bi^{3+} , or Sn 5s in Sn^{2+} , Pb 6s in Pb^{2+} and extended to higher energy levels. However, such a band engineering route by new phases is developed into another methodology and would not be discussed in this review.

Although the light absorption change is the most intuitive difference induced by the defects, it may not be the most important pattern of how the defects change the final PEC performance. In later paragraphs, the electronic impacts, particularly about the charge transfer and recombination are discussed.

3.2 Relationship with carrier transportation kinetics

Unlike photocatalysis, PEC system requires the electron (from anode) to flow all the way out from the SC to external circuit. Therefore, the photo-generated carriers must pass through the SC layer for hundreds of nanometers and even microns. Furthermore, the longer travel distance and much less surface area suggests the SC must be conductive enough to collect the current. Since the solar irradiation typically creates bonded electron-hole pairs rather than completely unchained free carriers, a large resistance will significantly increase the chance of those pairs to recombine via dissipation or photoluminescence. A fluent extraction of major carriers can notably facilitate the movement of minor carrier, namely holes in photoanodes, to the electrode-solution interface. In general, there are two factors related to the conductivity of the SC layer affecting the carrier transportation. The first one is still the crystallinity, for instance, the grain boundary scattering and all types of defects (not only point defects discussed in this section), changing the carrier mobility and lifetime; the second factor is the carrier density, which is determined by one or several specific type of defects in the SC. A suitable number of defects facilitate the major carrier transportation and benefits the photoelectrode with a larger photocurrent density, but an excess number of defects will act as recombination center that strongly trap all photo-generated carriers. Therefore, it is very important to control and optimize the defect level to achieve the best PEC performance.

Unfortunately, this optimized number is usually very hard to be predicted by modelling or computation. Experimental trial-and-error process is still the best and most straightforward method to figure out the optimized condition for a specific system. This optimization has been realized with various photoanodes, for instance BiVO_4 [64, 71, 72], SnWO_4 [73, 74], CuWO_4 [75, 76], with diverse approaches including doping with metal ions, hydrogen, and other elements, or controlling the intrinsic type of defects by post-synthesis activation procedures (i.e., thermal annealing, UV-curing, photo-charging, electrochemical treatment, etc.). These methods can improve the conductivity and thus benefit the PEC performance. Although it is very hard to predict the best level of de-

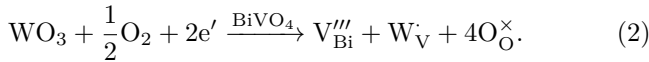
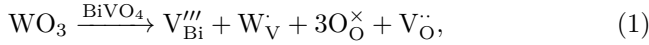
fects before test, the understanding of the speciation and concentration of defects is still helpful for elucidating photoanode property changes induced by the treatment mentioned above. In this section, we take BiVO_4 as an example to demonstrate how defects in SC layer were formed and the impact to the photoanode. The case can serve as a guiding paradigm to understand the defect in other oxide SCs.

In general, BiVO_4 is an promising candidate for PEC water splitting applications due to its good chemical stability, suitable VB edge position for OER and a theoretical maximum solar-to-hydrogen efficiency close to 10% [77]. However, its performance is limited by the hindered charge transport kinetics [72]. Due to its poor carrier mobility and a short carrier lifetime, the carrier diffusion length is limited to 70 nm [78, 79]. The short board between the transportation of electrons and holes can be discriminated by the illumination configuration. For the case of backside illumination, charge carriers are generated, on average, closer to the back contact and electrons have a shorter distance to travel, whereas the opposite is true for front-side illumination [80]. The photocurrent density of pristine BiVO_4 in back illumination is always much better than front illumination in numerous reports [18, 24], suggesting the electron transport is the limiting factor in those systems.

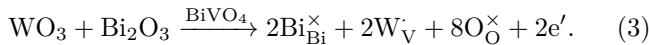
In another word, since electrons are the major carriers in the n-type BiVO_4 , increasing its electron density in CB can improve its electric conductivity and thus enhance its photoactivity despite the side effect of recombination. Given the flexibility of ternary oxide, doping is the most straightforward and controllable approach to control its carrier density via defects. The most commonly reported doping species of BiVO_4 includes high valence metal ions, i.e., Mo^{6+} , W^{6+} , which substitutes V^{5+} sites [34, 71, 81–85]. Specifically, a modest Mo^{6+} , W^{6+} doping act as donor impurities for increasing the carrier density and reducing majority carrier transport limitations, which caused extensive carrier accumulation and recombination. On the other hand, the isovalent ions of Bi^{3+} such as lanthanide (Ln) group elements Sm^{3+} , La^{3+} , Yb^{3+} could also improve the conductivity of BiVO_4 [86]. Again, several other non-metal doping and reductive treatments were also reported to be beneficial to the carrier transport properties of BiVO_4 photoanode. Since the chemical origin of above mentioned techniques are distinctly diversified, they are discussed specifically in following paragraphs.

As we stated above, one of the most developed doping methods for improving the conductivity of BiVO_4 is using W^{6+} to substitute V^{5+} sites. Abdi *et al.* [81] reported that 1% W-doped BiVO_4 could boost the carrier density, thus resolve poor carrier transport limitation, which could improve the photocurrent density to 2.3 mA/cm² compared to ~1 mA/cm² without doping. Moreover, the greatly enhanced electronic conductivity erased the photocurrent difference between front- and back-illumination,

suggesting the carrier transportation in SC layer was no longer the limiting issue. In addition, they suggested that the increment of carrier density attribute to W^{6+} substituting V^{5+} doping. If WO_3 was solely doped to $BiVO_4$, as shown in Eq. (1), The process is thermodynamically not favorable. In addition, Path (2) [see Eq. (2)] even reduces the electron density:



To compensate the adverse impact of solely having WO_3 in above reactions, more Bi^{3+} need be brought in the structure as well [24, 72, 87]:



The inference could be deduced from Eq. (3) that W^{6+} substituting V^{5+} sites results in net positive charges. It has to be balanced by free electrons that increases the carrier density, improves the conductivity and enhances the PEC performance.

In another report, the V_O^\cdot occurrence and contribution in annealed $BiVO_4$ was confirmed [84]. Its speciation can be written as [24, 84]:



Since the reaction involves oxygen in the chemical equilibrium, annealing in different atmosphere can lead to different contents of V_O^\cdot . A lower oxygen partial pressure yields a higher concentration of V_O^\cdot . The relationship could be calculated by defect equilibria and Brouwer diagram. Specifically, to their sample [84], the air-annealed sample have a higher electron density of $6.1 \times 10^{20} \text{ cm}^{-3}$ in contrast to $4.8 \times 10^{20} \text{ cm}^{-3}$ for O_2 -annealed sample.

Mo-doped $BiVO_4$ was also widely studied in recent years [5, 65, 82, 85, 88]. The function of the substitution of V^{5+} with Mo^{6+} is similar to that with W^{6+} , which could primarily improve the conductivity and decrease the surface carrier transportation barrier of photoanodes. However, Mo^{6+} doping works better than W^{6+} [89]. Nair *et al.* [85] has reported a Mo-doped $BiVO_4$ having impressively improved carrier separation efficiency. The photocurrent density of front- and back-side illumination in sulfite oxidation are similar and is 10 times bigger than that of undoped sample. The amendment was explained by the carrier transportation kinetics that, first, the electron mobility was significantly amended, and second is the prolonged carrier life time. For instance, a 4-fold improvement of the carrier mobility and the 200-fold of electron lifetime increment than pristine $BiVO_4$ for Mo-doped $BiVO_4$ films was reported by Seabold *et al.* [90]. Mo-doped $BiVO_4$ with reduced space charge layer thickness can significantly improve electron-hole separation and collection by drifting, which is the dominating movement of carrier in biased condition [85, 91]. Moreover, another plausible

possibility is that Mo sites can passivate traps and recombination centers at grain boundaries and perhaps also at the $BiVO_4$ /electrolyte and $BiVO_4$ /FTO interfaces, so that reducing not only the bulk recombination, but the interfacial one as well [85, 92].

The isovalent ion doped $BiVO_4$ in Bi^{3+} sites were reported in numbers of cases as well. As shown by a typical one reported by Govindaraju *et al.* [86], in Mott-Schottky plots, the Sm and Yb doped sample shows a more sluggish slope than pristine, suggesting their higher carrier density than pristine $BiVO_4$. Meanwhile, both the photocurrent densities increased in Sm- and Yb-doped $BiVO_4$. Combining experimental and theory calculation, the results showed these doping induced V_O^\cdot in bulk, which serves as donors and contributes to higher carrier density.

The doping level does not need to be uniform in the SC layer. For instance, gradient doping is a promising method for improving the charge separation efficiency of $BiVO_4$. Such a route has been reported by Abdi *et al.* [93] by introducing a gradient in the dopant profile, it is possible to create a distributed n^+ - n homojunction in $BiVO_4$. It not only optimizes the carrier density for efficient charge transportation, but also leads to a better charge separation efficiency by creating a wider space charge region. A separation efficiencies up to 80% are achieved. In addition, the aforementioned host scaffold components (WO_3) of Host scaffold-guest absorber structure have the similar function in some extent [31, 36].

The carrier transportation in $BiVO_4$ photoanode via other mechanisms rather than direct drifting or diffusion were observed as well, for instance, by bonded state and small polarons hopping [65, 78, 80, 94–97]. Recently, a rising trend is to improve the charge mobility by promoting small polarons hopping pathway. Zhang *et al.* [96] have observed the phenomenon that, the photocurrent density of Mo-doped $BiVO_4$ photoanode increase from 1.8 mA/cm^2 to 4.0 mA/cm^2 followed by temperature elevating from 10°C to 42°C , the fill factor also increase distinctly. The mobility increased along with elevated temperature corresponding to stronger small polarons hopping in SC [98]. Combined with theoretical calculation, the polarons intermediated transport mechanism of Mo-doped $BiVO_4$ was proposed by Zhang *et al.* [95]. An additional electron is placed at V sites and form the $V^{4+}O_4$ small polarons, the V-O bond in $V^{4+}O_4$ is longer than $V^{5+}O_4$, which implies strong electron-phonon coupling in this small polarons hopping process. A $Mo^{6+}O_4$ unit with positively charge and small polarons $V^{4+}O_4$ unit with negatively charge attract each other electrostatically, which decrease electron transport efficiency in some extent. However, The volume both of unit $V^{4+}O_4$ and $Mo^{6+}O_4$ are bigger than $V^{5+}O_4$, which forces them to be separated easier for less local structural distortion and a lower energy in crystal, this volume effect is superior to electrostatic attract interaction in carrier transport process. Therefore, a volume effect decreases electron transport path and provides

a lower barrier for electron hopping. The small polarons mobility and photocurrent density was boosted by extrinsic dopants, which provide the new insight into doping for improving the photoanode properties.

In comparison with doping using other elements, hydrogen can be much more complicated than just as a dopant. The hydrogen annealing process has been proved a quite universal way to improve the conductivity and PEC performance of n-type oxides. Even for binary oxides, the mechanism of its impact is not fully clear yet and highly diversified to different oxides [41, 80, 97, 99–102]. Nonetheless, this method creates various interesting functionalized materials. As abovementioned, H₂ atmosphere annealing of pristine TiO₂ lead to the formation of black TiO₂ [41]. Such a distinct difference from hydrogenation treatment drew great attention of researchers, and was used for not only for aforementioned better light absorption, but also improving the conductivity and the carrier transport efficiency of various SC photoanodes [34, 80, 97, 103, 104], such as WO₃ [105, 106], TiO₂ [42, 60], BiVO₄ [34, 80], CuWO₄ [101, 107], and Fe₂O₃ [102].

Cooper *et al.* [80] reported the performance improvement of BiVO₄ after annealing under hydrogen atmosphere, which induced the formation of H interstitial

(H_{int}) and H substitute the O sites (H_O) into BiVO₄. The majority carrier transport limitations can be observed from the PEC properties in As-grown sample, As shown in Fig. 7(a), the photocurrent density of back-side illumination is 2.6 mA/cm² contrast with 1.6 mA/cm² in front-side illumination at 1.23 V vs. RHE, consisting with others reports [72, 85]. In contrast, after annealing in hydrogen at 275 °C, the photocurrent density of front-side illumination increased distinctly rather than back-side illumination, indicating the removal of limiting factor to major carrier transportation. In addition, the onset potential and fill factor were improved. On ¹H-NMR spectra [see Fig. 7(b)], peaks at 0.2 ppm and 7–9 ppm introduced by hydrogen annealing were assigned to H_O and H_{int} respectively. Further, the content of V⁴⁺ increased as well. These V⁴⁺O₄ sites are small polarons and proposed as the dominant contributor to the major carrier concentration. Increasing the annealed temperature from 245 °C to 290 °C tuned the Fermi energy of samples from 0.49 to 0.44 eV below E_{CB} [see Fig. 7(c)], and an upward displacement of Fermi level due to the carrier concentration increased. The attraction between small polarons with negative charge and positively charged V_O[•] results in bound polarons, whose mobility is worse than unbound

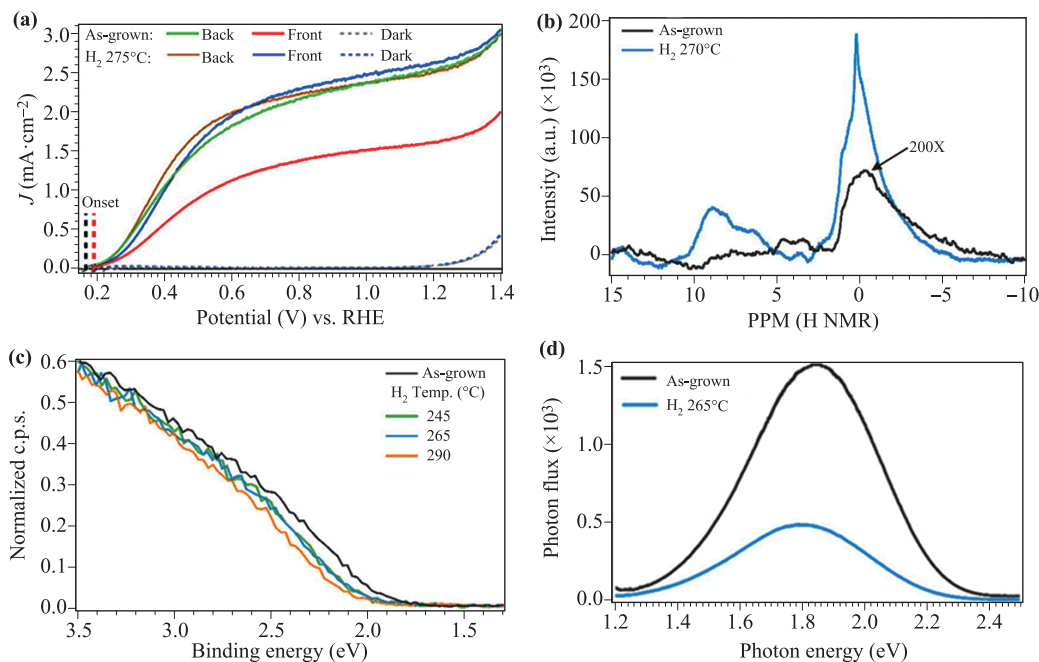


Fig. 7 (a) PEC testing of nano-BiVO₄ samples in 0.5 M phosphate buffer with 1 M Na₂SO₃ (pH 7.16), deposited on FTO/glass substrates, showing the forward sweep of the second cycle from open-circuit voltage to 1.4 V vs. RHE. The E_{on} is shown for the H₂ annealed sample, which yielded the lowest value of 167 mV. As-grown films are compared to films annealed in hydrogen at 275 °C. (b) ¹H-NMR of BiVO₄ powder As-grown (gray) and H₂ annealed at 270 °C (blue). The signal from the As-grown sample is magnified 200× for ease of comparison. The signal at ~7–10 ppm is consistent with interstitial hydrogen, and the signal at ~0 ppm is assigned to substitutional hydrogen. (c) Valence band spectra of As-grown BiVO₄ (gray) and BiVO₄ that was H₂ annealed at 245 °C (green), 265 °C (blue), and 280 °C (orange). Measurements were performed on BiVO₄ thin films on FTO glass substrates and indicate a progressive shift of the Fermi energy toward the conduction band edge with increasing H₂ annealing temperature. (d) Temperature-dependent photoluminescence (PL) Spectra taken at 20 K are shown for As-grown (gray) and H₂ annealed at 265 °C. Reproduced from Ref. [80], Copyright © 2016 American Chemical Society.

polarons created by self-trapping (H_O or H_{int}) of photo-generated charge carriers. Temperature-dependent photoluminescence (PL) spectroscopy also revealed a lower radiative recombination (deep trap states associated with V_{O}^{\cdot} defects) in H_2 -annealing sample than as-grown BiVO_4 . Therefore, in BiVO_4 samples, all experimental proofs suggest that, although both related to a lower O content, only the hydrogen incorporated defects rather than V_{O}^{\cdot} formation in the structure is beneficial to the PEC performance.

The hydrogen annealing process is applicable to other n-type ternary oxides. Similar to BiVO_4 , CuWO_4 photoelectrodes also suffer from the low charge separation efficiency in bulk [98]. Hu *et al.* [108] reported a better photocurrent density of CuWO_4 film by hydrogen-treatment from 0.7 mA/cm^2 to 1.0 mA/cm^2 . 3.5% of W^{6+} was reduced to W^{5+} revealed by X-ray photoelectron spectroscopy (XPS), which corresponds to the formation of V_{O}^{\cdot} . The author proposed V_{O}^{\cdot} as shallow-donors for higher carrier density, which is 2.7-fold of untreated sample. In addition, Tang *et al.* [101] also reports that a larger current density of H-treated CuWO_4 samples, with carrier density is 3.5-fold than the control. Similar reports also have been discovered in MgFe_2O_4 and CuFe_2O_4 with those of ZnFe_2O_4 [100, 109]. However, due to the experimental difficulty of characterizing hydrogen atoms, particularly as a dopant with low content, usually it is very hard to discriminate the true contribution is from either the simple oxygen vacancy or hydrogen occupied sites. Even though, experimental trials of hydrogen treatments to n-type oxides are always worth to try, and the optimized conditions can be empirically determined.

Electrochemical methods were also feasible to create defects beside abovementioned routes of doping in the synthesis or via thermal infusion from gas phase. An electrochemically reduction approach of doing that was reported by Wang *et al.* [110] which can improve the conductivity of BiVO_4 . The BiVO_4 photoanode was reduced in mild condition and brought out a photocurrent density of 10-folds higher than the pristine BiVO_4 . They proposed the remarkable improvement was probably due to the V_{O}^{\cdot} , which is result of the reducing V^{5+} and Bi^{3+} to lower valence state, this phenomena also be observed in Ref. [11].

It is worthy to note that the doping level is not the higher the better. Usually an over-doped sample could still have good conductivity, but much shorter carrier diffusion length due to strong scattering effect of carriers. Furthermore, the defects can also act as recombination centers which result in deteriorated PEC performance, i.e., lower onset potential and smaller photocurrent density, in the next section, the negative effect will be discussed in detail.

3.3 Acting as recombination centers

In above paragraphs we discussed the constructive contribution of defects to SC photoanodes. However, using defects is a double-edged sword, which may also degener-

ate photoanodes as recombination centers which eliminate electron-hole pairs. The crystal defect may have deep energy level in bandgaps which traps electron or/and hole, decreasing the carrier lifetime. Indeed, almost all defects could serve as recombination centers, such as vacancies, impurity atoms and self-interstitial atoms.

For instance, Abdi *et al.* [72] reported that W_V serve as electron traps decreasing the carrier lifetime and mobility for an order of magnitude. Its speciation can be written as Eq. (5):



In addition, the carrier tend to be located and form polarons decreasing the carrier transport efficiency as we discussed above [97]. Therefore, the efforts for avoid or at least reduce the undesired defects in SC are as important as to improve the SC photoanode via “good” defects. Various approaches has been used to tame the doping into desired levels, such as using reasonable doping elements content [85, 96], control annealing temperature, time and atmosphere [5, 9, 62, 104], and the redox chemistry of the elements [11, 110] in the SC. Given the chemistry and physics of these parameters are so diverged, we focus our discussion to the performance aspects caused by above processes.

The PEC performance varied with the doping concentration was reported widely, such as W^{6+} , Mo^{6+} -doped BiVO_4 [81, 85, 111–113], Si, Mg-doped TiO_2 [114, 115], Ti^{4+} , Si^{4+} , Sn^{4+} -doped Fe_2O_3 [20, 92, 116], Fe-doped CuWO_4 [75], and Ti^{4+} -doped ZnFeO_4 [117]. Taking our previous work as an example, impacts of Mo doping on BiVO_4 PEC performance differed distinctly at different doping levels. With Mo doping lower than 0.3 at.%, the photocurrent increased along with Mo content; but for doping concentrations between 0.3–1 at.%, the photocurrent decreased with higher Mo level. Such an observation can be roughly explained that excessive dopant served as the recombination centers [see Fig. 8(d)].

The intrinsic defects usually can be described with crystallinity and its influence on the PEC performance has been extensively examined [5, 8, 118–122]. However, the exploration on crystallinity issue is sometimes limited by the overall photoelectrode structure, for instance, the ITO or FTO glass substrate. The particle transfer protocol nicely bridged the variance of synthesizing SC material themselves and the requirement of making good contact of powders with the substrate [5, 67, 123, 124]. Using this route, we explored the SC crystallinity changes during post-annealing in different temperature and that influence on the PEC performance. As shown in Fig. 8, the photocurrent density increased with BiVO_4 prepared from 450°C to 800°C although particles grown larger simultaneously. The better crystallinity along with elevating temperature [see Fig. 8(b)] produced better performance, indicating the crystallinity suppressed the drawback brought by sintered particles. Meanwhile, the crystalized structure

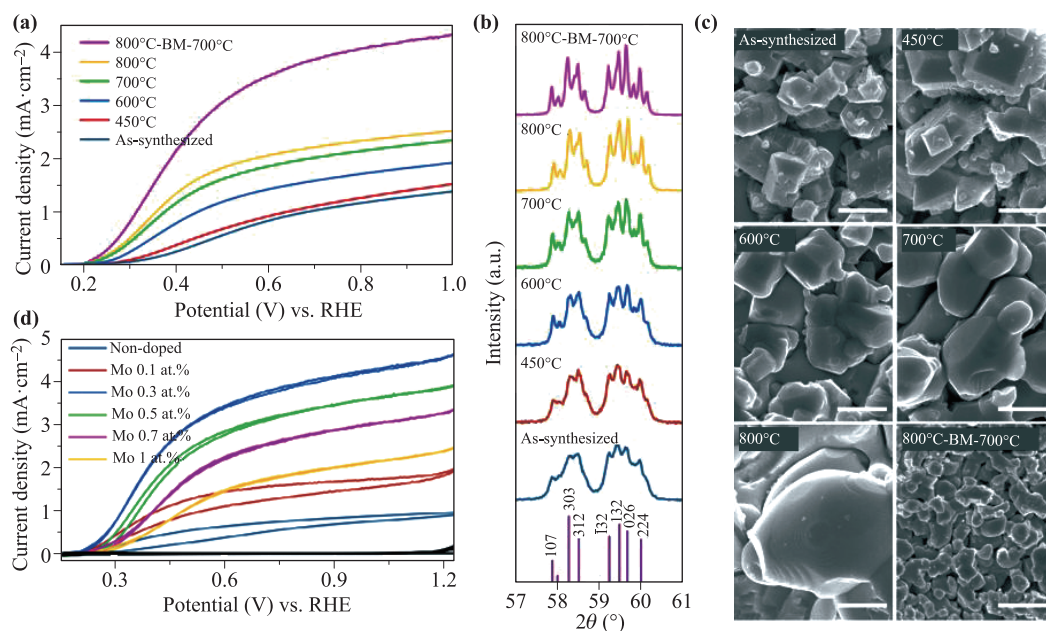


Fig. 8 Characterization of bare 0.3 at.% Mo-doped BiVO_4 electrodes. **(a)** Current–potential curves for sulfite oxidation in 0.2M sodium sulfite containing 1M potassium borate buffer at pH = 9 under AM 1.5G irradiation comparing the charge separation abilities of bare Mo-doped $\text{BiVO}_4/\text{Ni}/\text{Sn}$ electrodes prepared using As-synthesized particles, particles annealed at various temperatures (as shown in the legend), and particles treated by 800°C annealing followed with ball milling and 700°C post-annealing (800°C-BM-700°C). **(b)** Narrow-range XRD patterns of the same set of Mo: BiVO_4 particles. The standard XRD pattern for monoclinic BiVO_4 is shown at the bottom (JCPDS, No. 83–1699). **(c)** SEM images of the same set of electrodes. Scale bars, 1 μm . **(d)** Effect of Mo-doping contents on the photoelectrochemical properties of bare Mo: $\text{BiVO}_4/\text{Ni}/\text{Sn}$ electrodes. CV curves of BiVO_4 particle electrodes prepared from particles with Mo doping concentrations between 0–1 at.% were recorded for sulfite oxidation under AM1.5G irradiation. The black curves are the corresponding dark currents. All BiVO_4 particles were treated by 800 °C annealing, ball milling and 700 °C post annealing sequentially. Fitted lines added as a guide to the eye. Reproduced from Ref. [5], Copyright © 2016 Nature Publishing Group.

also reduced the chance of photo-corrosion that comparing to nanoworm BiVO_4 . It is noteworthy that the annealing process is affecting various aspects of the materials rather than only reducing defects, for instance, it could result to sintering, evolving of new defects, phase transformation, surface reconstruction and even sublimation. Therefore, it is tricky but necessary to carefully consider above mentioned possibilities and extract the true contribution from the key factors behind phenomenological explorations.

A mild reductive condition may anneal the BiVO_4 with larger improvement. The mechanism of this annealing was not completely clear yet, for instance, in above discussion the improvement was mainly attributed to the hydrogen substituted or interstitial sites. However, in another case reported by Jang *et al.* [97], they proposed an explanation based on the elimination of undesired defects. As shown in Table 2, the photocurrent density of hydrogen treatment BiVO_4 is increased 25% compared to pristine BiVO_4 with the onset potential shifted 100 mV lower. The carrier lifetime and carrier diffusion length both increased about 2-folds than pristine BiVO_4 . On the contrary, the carrier lifetime and diffusion length is decreased in W-doped BiVO_4 than pristine BiVO_4 , the result was explained with the recombination centers formed

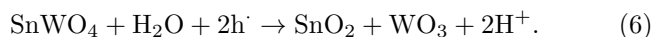
at W_V defect sites in W-doped BiVO_4 . They also observed the hydrogen contents increased significantly in hydrogen treatment sample. Time-resolved microwave conductivity (TRMC) shows the trap states appearing after hydrogen treatment. In the meantime, the lower sub-bandgap photoluminescence intensity represents the trap state reduction. Thus, the reduction in the number of trap states was consistent with the increase in carrier lifetimes. Combining experiment and theory calculation, they proposed the formation energy of interstitial vanadium ($\text{V}_\text{i}^{\bullet\bullet}$) and vanadium antisite on bismuth ($\text{V}_\text{Bi}^{\bullet}$) in lower than others in untreated BiVO_4 , which means both defects are easier to form. However, the formation energy increased in both defect by insertion hydrogen, therefore, the hydrogen treatment diminished the trap states and passivated the lattice, which benefited the carrier lifetime and diffusion length. Therefore, although the mechanism of improved PEC performance by hydrogen annealing is not detailed yet, experimentally such a method is quite useful for achieving high performance photoanode.

The statement of eliminating undesired defects in the bulk SC sounds always right for photoanodes. However, the problem is what it is very hard to figure out the impact of different defects in the bulk, particularly in some

Table 2 Carrier mobilities, lifetimes, and diffusion lengths of pristine, hydrogen-treated, and 1% tungsten-doped BiVO₄ [97]. (μ : Carrier mobility, μ_e : Electron mobility, μ_h : Hole mobility, τ : Carrier lifetime, L_h : Carrier diffusion length, N_d : Carrier density) All values were measured using a 355 nm laser pulse with a photon flux of 1.65×10^{12} photons cm^{-2} pulse⁻¹.

Photoelectrode	μ ($\text{cm}^2 \cdot \text{V}^{-1} \cdot \text{s}^{-1}$)	μ_e ($\text{cm}^2 \cdot \text{V}^{-1} \cdot \text{s}^{-1}$)	μ_h ($\text{cm}^2 \cdot \text{V}^{-1} \cdot \text{s}^{-1}$)	τ (ns)	L_h (nm)	N_d (cm^{-3})
Pristine BiVO ₄	0.07	0.04	0.03	43	57	$7.0 \pm 1.7 \times 10^{18}$
H-BiVO ₄	0.08	0.045	0.035	109	101	$1.1 \pm 0.3 \times 10^{21}$
W-BiVO ₄	0.02	0.01	0.01	32	28	$2.9 \pm 0.8 \times 10^{21}$

defect-rich or nonstoichiometric structures. For instance, α -SnWO₄ with 1.64 eV bandgap that cross the redox potential of water [73, 125–127] and has been regarded as a promising photoanode materials. However, based on the experiment of Zhu *et al.* [73], its performance was strongly limited by the bulk defects. The porous α -SnWO₄ film prepared by a hydrothermal conversion of WO₃ film only produced a photocurrent density far below the theoretical number estimated from the bandgap width. The film was tested in both nonaqueous and aqueous electrolyte solutions, with performance barely changed. Sn⁴⁺ was detected on the surface after aqueous test, which mechanism is mentioned as below:



Such an oxidation did not take places in nonaqueous environment, indicating the surface Sn²⁺ oxidation is not the limiting factor. The incapability of hole scavenger Na₂SO₃ towards its PEC performance also agreed with above consideration. Besides, the anode transients became more obvious in present of the hole scavenger than it absent. This phenomenon may be resulted from localized or trapped charge within the bulk. Based on both experiment and modelling, they propose Sn antisite at W, Sn_w^{'''} defect could formed easily in Sn-rich and W-poor synthesis condition, which play as the deep, localized hole trapping states. Thus, the Sn_w^{'''} defect may correspond to small polaron conduction similar to the scenario of BiVO₄ as we mentioned above. However, since the α -SnWO₄ photoanode was not extensively studied like BiVO₄ or TiO₂ yet, both the experimental facts and related characterization are far from sufficient to illuminate the impact of defects in this structure. Therefore, the exploration of reasonable synthesis conditions is even more desired for α -SnWO₄ photoanode, particularly if it is well designed to illustrate the specific role of a certain type of defects.

4 Interfacial states between semiconductor and electrolyte solutions

The interface is the boundary condition for a piece of SC in solid physics. On this layer, the lattice lost its translation symmetry and result to new electronic and chemical states that do not exist in the interior part. For PEC system, these states decide the interface characteristics between

SC surface and electrolyte solutions. Since the dangling bond cannot exist on a real surface in solution, the interaction between SC and solution results to surface states via various mechanisms, such as lattice imperfection, impurities ion absorption, doping, SC surface species redox, photocorrosion and chemical dissolution during PEC test. The existence of interfacial states is a double-edge sword with both two sides. The positive effects mainly include serving as catalytic active sites, and modulating the surface hydrophilicity, improving the carrier separation and transfer efficiency, etc.. The negative effects are such as serving as recombination centers, formation of Fermi Level Pinning, and complication to the design of multilayered structure. Both the pros and cons are discussed in this section based on the mechanism, from the aspect of improving their electrochemical activity, charge transfer kinetics, band position (Fermi level pinning) and stability. The discussion is based on several popular photoanode SC materials as the examples, for instance, TiO₂, BiVO₄, and Fe₂O₃.

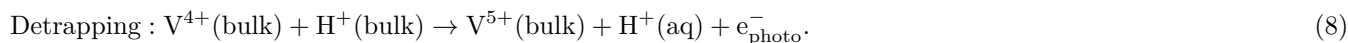
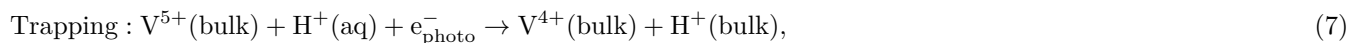
4.1 Surface active sites for electrochemical reaction

Almost all typical n-type oxide SCs are not good electrocatalyst for OER reaction. This is not surprising since the electrocatalytic materials have electronic structural requirements that dramatically different with the band structure for good PEC materials. In the cases of photoanode with bared SC surface, the presence of defect can provides electrocatalytic pathways for the photogenerated holes to flow out of the SC. Namely, the defect works as electrocatalytic sites and also become the new limiting factor on surface to the overall efficiency of the photoelectrode. The evolvment of these type of defects is not rare and has been spotted with many SCs, such as Ti³⁺ in TiO₂ layer [40, 128–130], V_o in α -Fe₂O₃ [131], V_o in W-doped BiVO₄ [84], and quasi-V_o in Mo-doped BiVO₄ [82]. However, in most cases they are a serendipitous benefit from the interface rather than rationally designed structure.

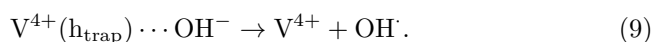
Different surface states may coexist on the same electrode. To promote the formation of beneficial or at least neutral defect would be important and helpful to the PEC performance. For instance, the electron trapping states on surface can be categorized into surface charge transportation and recombination centers. The W-doping to BiVO₄ lead to the concentration and ratio between these two types of surface states changed [112]. Using the W-doped

BiVO₄ photoanodes fabricated by electrospinning as the model, their correlation can be investigated by cyclic voltammetric (CV) studies. Based on the observation, they proposed the different roles of defects in the process. The evolution of surface states associates with different W-doping level was showed in Fig. 9. A reversible redox

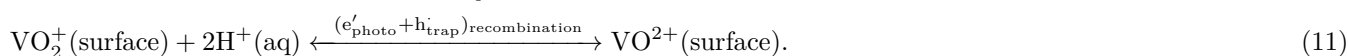
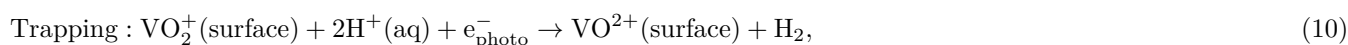
peak at 0.8 V_{RHE} Corresponding to V⁴⁺/V⁵⁺ in BiVO₄ was observed. This redox process was significantly larger upon illumination, and the current density response to the increasing scan rate positively, which indicate V⁴⁺/V⁵⁺ as a reverse redox couple on BiVO₄ surface, it can be written as Eq. (7) and Eq. (8):



V⁴⁺ induces the formation of the V_O on the surface, which enhances the hole transfer through the interface via Eq. (9):



On the other hand, the presence of oxo-V defects, VO₂⁺/VO²⁺, trap electrons easily but difficult to detrapp, and then increasing the chances recombination, it can be written as Eq. (10) and Eq. (11):



Only a suitable concentration of doping could balance the required high concentration of V⁴⁺ sites and suppress the presence of oxo sites. Similar issue was reported in another case of W-doped BiVO₄ by Zhao *et al.* [84]. The V_O plays as active sites in porous W-doped BiVO₄. The samples went through different annealing atmosphere and gave a response of better carrier transport efficiency through the interface with higher V_O content.

The active sites with oxygen vacancies can be observed with more details in some classical model systems. For instance, by comparing pristine and reduced anatase TiO₂(001) surface with XPS and scanning tunnelling microscopy (STM), Wang *et al.* [128] observed the correlation of oxygen and water adsorption associates with the

distribution of Ti³⁺. The spectroscopy-microscopy coupled study clearly proved the Ti³⁺ defects are the primary binding sites for H₂O and O₂. Even such an observation may not exactly represent the true condition of photoanodes, the concept of understanding the interesting chemical sites is very helpful.

It is well known that the hydroxyl groups have a great impact to the charge distribution in the double layer region of the SC electrode, thus may change their band bending and other important features [132–134]. For instance, various methods was reported for generating a large amount of surface hydroxyl on TiO₂ surface, such as UV treatment [135], plasma etching [136], Hydrogen-annealing [99], and Ammonia-induced reduction [132]. In

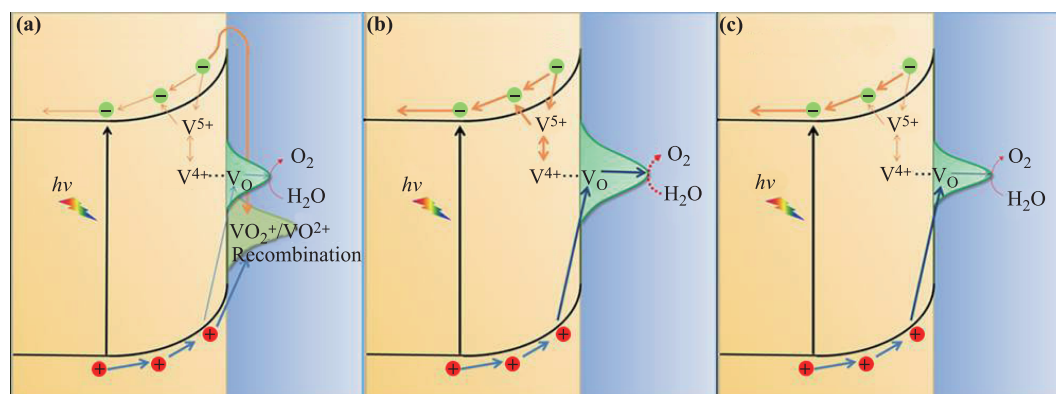


Fig. 9 Schematic illustration of the proposed mechanism as a function of the W doping level: low (a), middle (b), and high (c); the thicker the arrow, the faster the process. Reproduced from Ref. [112], Copyright © 2018 American Chemical Society.

above literature, the performance of TiO_2 photoanode with hydroxyl-rich surface was improved than their control to an extent. The phenomenon could be interpreted that relating to surface-states acting as hole traps to form new radical [132, 137]. And more importantly, the trapped positive charge can be effectively used in water oxidation, namely the surface states are actuarially acting as catalytic sites promoting the water oxidation [135] with prolong the hole lifetime [132, 138], as shown in Eq. (12):



OH_S formation has been evidenced by diffuse reflectance infrared Fourier transform spectroscopy (DRIFTS) [138, 139] and electron paramagnetic resonance (EPR) spectroscopy [140], Terephthalic acid (TPA) fluorescence probing [141], etc.. In addition, density functional theory (DFT) calculation also predicted the photo-generated hole combined with OH_S^- to form OH_S [142, 143]. Therefore, it is not very hard to interpret that even with similar density of hydroxyl groups on the surface, the activity can be very different responding to the pH of the electrolyte solution.

It is worthy to note that, although these sites are beneficial to the electrochemical steps, their presence might not be necessary for a good photoanode. The reason is quite simple that these sites are better than nothing, but still not competitive to those well-designed electrocatalyst for anodic reactions. In such a circumstance, the design concept changed from bridging the holes with water oxidation directly to link it with the suitable electronic state of the electrocatalyst. Also, avoiding the undesired defects will be still necessary for the efficient charge transfer through the interface rather than recombination.

4.2 The Fermi level pinning by surface states

The surface states widely exist on all interfaces, but in the context of photoelectrodes the term usually refers to redox active surface states which could easily withhold the charge carrier produce by the SC bulk. Such interfaces can be commonly seen with several metal oxides, such as BiVO_4 [66, 79, 112], Fe_2O_3 [144–146], MFe_2O_4 ($M = \text{Cu, Mg, Zn}$) [100, 118], and even metal oxo-nitrides BaNbO_2N [118] and nitrides (Ta_3N_5 [147–149]). The high density of surface states trap the carriers and act as the recombination centers [see Fig. 12(b)]. The charging of these states leads to Fermi level pinning and anodic shift of onset potential, which is destructive to the photoanode [79, 150, 151]. Herein, we briefly discuss about these impacts using Fe_2O_3 and Ta_3N_5 photoanodes as examples.

Surface states on Fe_2O_3 are mainly the result of oxygen vacancies and hydrolyzation. The resulted Fe^{2+} in oxygen deficient regions (V_O^\bullet) [145, 152–154] forms $\text{Fe}^{2+}/\text{Fe}^{3+}$ redox couples acting as the recombination centers for holes trapping during charge/discharge process [145]. Furthermore, these surface states usually lead to Fermi-level pin-

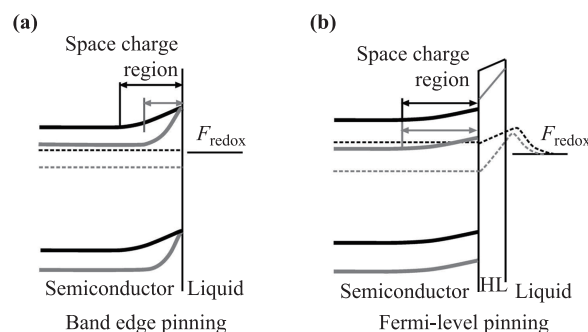


Fig. 10 (a) Under band-edge pinning condition (ideal condition), the degree of band bending enlarges with enhanced applied electric bias and the band position of the SC at the SC/liquid interface remains unchanged. (b) Under Fermi-level pinning conditions, the degree of band bending remains unchanged and the applied bias drops within the Helmholtz layer (HL). The gray and black lines in (a) and (b) are under different bias. The bumps between SC and liquid in (b) represent potential drop in HL. Reproduced from Ref. [155], Copyright © 2013 Elsevier.

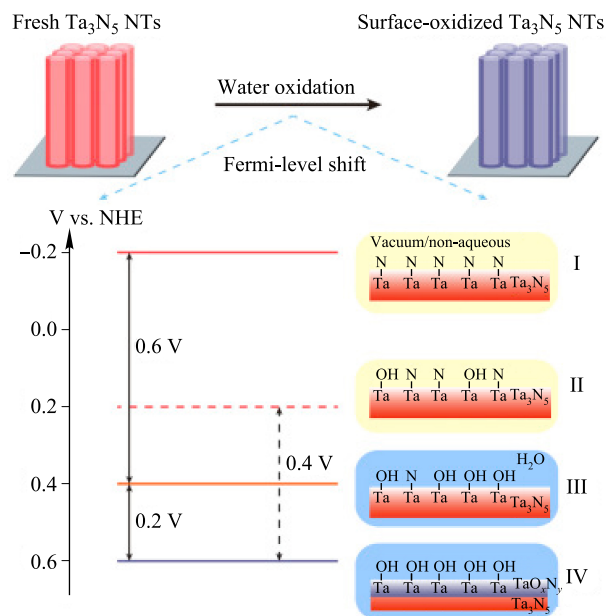


Fig. 11 The Evolution of Ta_3N_5 Surface Energetics: Stage I: fresh Ta_3N_5 free of H_2O . Stage II: Ta_3N_5 with partial H_2O adsorption due to exposure to ambient air. Stage III: Ta_3N_5 immersed in H_2O . Stage IV: Ta_3N_5 with surface oxides. The horizontal lines correspond to the surface Fermi-level position of Ta_3N_5 in stages I–IV. Reproduced from Ref. [147], Copyright © 2016 Elsevier.

ning (see Fig. 10), making the applied bias barely changes the band bending which is required by the carrier drifting. In this scenario, the photocurrent become strongly limited and gives a notable retarded transient response.

Ta_3N_5 is another material severely suffering from the surface states, as the result of a self-limiting surface oxidation during the PEC test. He *et al.* [150] have reported

their observation of the oxide amorphous layer on the surface gradually grew to 3 nm upon prolonged testing time. The phenomenon was also reported in other recent works [148, 149, 156]. The defective oxide layers on Ta_3N_5 surface lead to significant charge recombination and act as an insulating layer which reduce the charge transfer across the photoanode/electrolyte interface. The high density of surface states resulted in Fermi-level pinning as well, which fatally affects the photovoltage and stability. The degree of Fermi-level pinning corresponds to the oxidation content in Ta_3N_5 surface, as shown in Fig. 12. Efforts were necessary to be made to alleviate this surface oxidation.

4.3 Surface-state passivation

Given many SCs with suitable band structure do not have the suitable and stable surface for electrochemical reaction, it is a better idea to completely cover the surface with other functionalized materials, namely the passivation layer and electrocatalysts. As we discussed in the previous section, the surface states lead to PEC properties decreasing. Thus, the surface state passivation is an effective strategy to improve the performance of photoanodes.

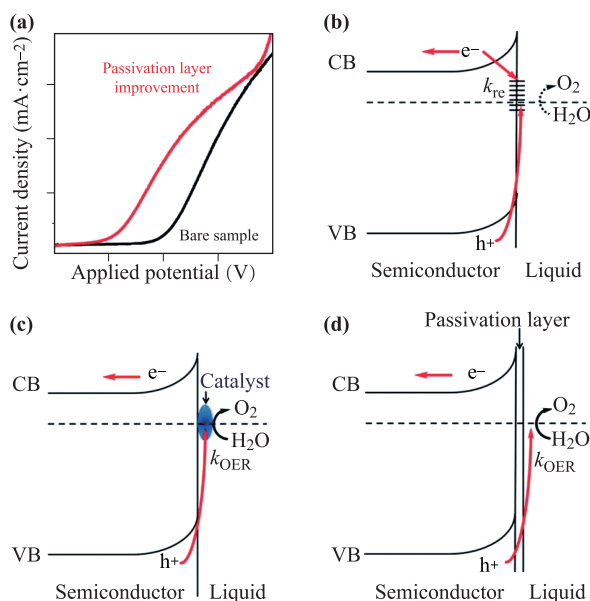


Fig. 12 Comparison of an n-type SC photoanode and the effect on surface states with/without a passivation layer in a water-splitting PEC cell: (a) the schematic J - V curves of a photoanode with (red trace) and without (black trace) (a) surface passivation layer; (b) surface defect states in the band structure, which lead to high charge recombination and inefficient water oxidation by the photogenerated holes; (c) application of an OER catalyst layer, which promotes facile hole transfer across the interface to the catalyst for improving water oxidation; (d) application of a thin noncatalytic surface layer to passivate defect states, strongly suppressing surface recombination for improving water oxidation. Reproduced from Ref. [163], Copyright © 2014 Royal Society of Chemistry.

Herein, we discuss several typical functional overlayers, for instance, as depicted in Figs. 12(c, d), including cocatalysts (electrocatalysts) and passivation layers.

As we stated above, the existence of electrocatalyst/cocatalyst is usually more effective than only using surface states as the intermediates for anodic reactions. Loading oxygen evolution cocatalyst on Fe_2O_3 effectively extracts the holes by providing suitable energy states to reduce recombination and accelerate the surface reaction [146] [see Fig. 12(c)]. Typical cocatalysts include Co-Pi [157–159], IrO_x [160], NiFeO_x [161], etc.. For instance, Zhong *et al.* [159] have described that the Co-Pi cocatalyst film prepared by photo-assisted electrodeposition on to mesostructured α - Fe_2O_3 photoanodes. The photocurrent onset potential shifted -170 mV, which suggest that the Co-Pi cocatalyst greatly eliminated the electrochemical polarization. Klahr *et al.* [158] reported ALD grown Fe_2O_3 film with Co-Pi cocatalyst layer of different thickness by photo-assisted electrodeposition. The negative shift of onset potential increases with Co-Pi film thickness. The charge collecting and storing properties of Co-Pi cocatalyst was studied with electrochemical impedance spectroscopy (EIS), suggesting the Co-Pi cocatalyst enhances carrier separation and prevents the recombination on the surface. Furthermore, recent operando study by Tilley *et al.* [160] using potential-sensing electrochemical atomic force microscopy indicated the Co-Pi was charged by photogenerated holes from Fe_2O_3 during the PEC test until it reached a potential where Co-Pi-mediated water oxidation entered the steady-state and then drives water oxidation. The Co-Pi extracts holes from the SC layer and uses them in oxygen evolution reaction. However, the contribution of Co-Pi to photoanodes is somewhat controversial, regarding what is its primary role on the surface. Nonetheless, other electrocatalysts such as IrO_x [160] has similar improvement as cocatalysts which can reduce the surface recombination and lower the onset potential.

Since the cocatalyst layer may not be compact enough to completely protect the inner SC layer, a passivation layer is still preferred for photoanodes with stability over tens of hours. Besides serving as a separator between SC and solution, another important role of the passivation layer is to avoid the formation of surface recombination centers [see Fig. 12(d)]. Hisatomi *et al.* [144] have reported 13-group oxide layer (Al_2O_3 , Ga_2O_3 or In_2O_3) deposited onto the Fe_2O_3 , the Fe_2O_3 modified with Ga_2O_3 , the onset potential shifted -0.2 V and the photocurrent density increased at lower potential 1.2V vs. RHE. Using Al_2O_3 and In_2O_3 overlayers have similar effect in lowering the onset potentials. Similarly, Yang *et al.* [162] have deposited the ultrathin TiO_2 layer by Atomic Layer Deposition on the Fe_2O_3 film, the photocurrent onset potential shifted -0.1 V.

Besides a coating or deposition, a functional overlayer can be introduced by in-situ reactions of the SC during PEC tests. Hu *et al.* [145] reported the V_2O_5 closely related

to the surface state. The oxygen atoms are “covalently fixed” in phosphate (PO_4^{3-}), which suppresses the formation of V_O . Thus, the surface state was passivated efficiently and the onset potential was lowered by 0.15 V. The photocurrent density increased 4.2-fold compared to pristine Fe_2O_3 . The oxygen atoms on the surface are “covalently fixed” in phosphate anions, which inhibited the surface states and promoted the PEC performance.

New chemical bonds take place with the new interface between cocatalyst or passivation layer with the SC. For instance, He *et al.* [148] have observed that the Ta-O-Co bonding formed between $\text{Co}(\text{OH})_2$ and Ta_3N_5 under the PEC condition (see Fig. 13), which reduced the Fermi-level pinning effect. This phenomenon is similar to the above-mentioned covalent bond between phosphate and V_O in Fe_2O_3 . The onset potential shifted from 1.0 V to 0.8 V vs. RHE and the photocurrent density increased from 2.2 mA/cm^2 to 4.2 mA/cm^2 after the in-situ activation. The open-circuit potential (OCP) of $\text{Ta}_3\text{N}_5/\text{Co}(\text{OH})_2$ as measured in light shifted negatively due to PEC reactions by 0.14 V, indicating that the surface Fermi level shifted toward the conduction band edge. The intensity modulated photocurrent spectroscopy (IMPS) data clearly confirmed that the surface recombination rate constants (k_{re}) at 0.9 V decreased by a factor of 3 when the PEC treat-

ment was extended from one CV scan to 20 min photoelectrolysis. In addition, the stability was elevated to over 150 min compared to the freshly-prepared one with 60 min. Those phenomena indicated that the Fermi-level pinning was lifted by Ta-O-Co bonded interaction, with reduced surface charge recombination as well as a better cross-interface charge transportation.

Liu *et al.* [156] reported that the surface state of Ta_3N_5 was passivated during the cooling-down process of synthesis by replacing NH_3 flow with a trace amount of O_2 containing Ar flow. This passivated sample is named $\text{Ta}_3\text{N}_5(\text{P})$ (see Fig. 14). The onset potential was lowered by 130 mV compared to the control sample. The photocurrent density increased to 2.5 mA/cm^2 compared to 1 mA/cm^2 at 1.23 V vs. RHE. Furthermore, after they removed this passivation layer with etchants, the photocurrent curve resembled the pristine Ta_3N_5 . Therefore, this case provides a paradigm of rational control of the side reactions during the preparation procedure.

Zhong *et al.* [164] reported that an effective GaN coating strategy is developed to remarkably stabilize Ta_3N_5 by forming a crystalline nitride-on-nitride structure with an improved nitride/electrolyte interface. Mott-Schottky plots results evidenced that the flat-band potential of $\text{GaN}/\text{Ta}_3\text{N}_5$ sample is 0.22 V vs. RHE, which was sig-

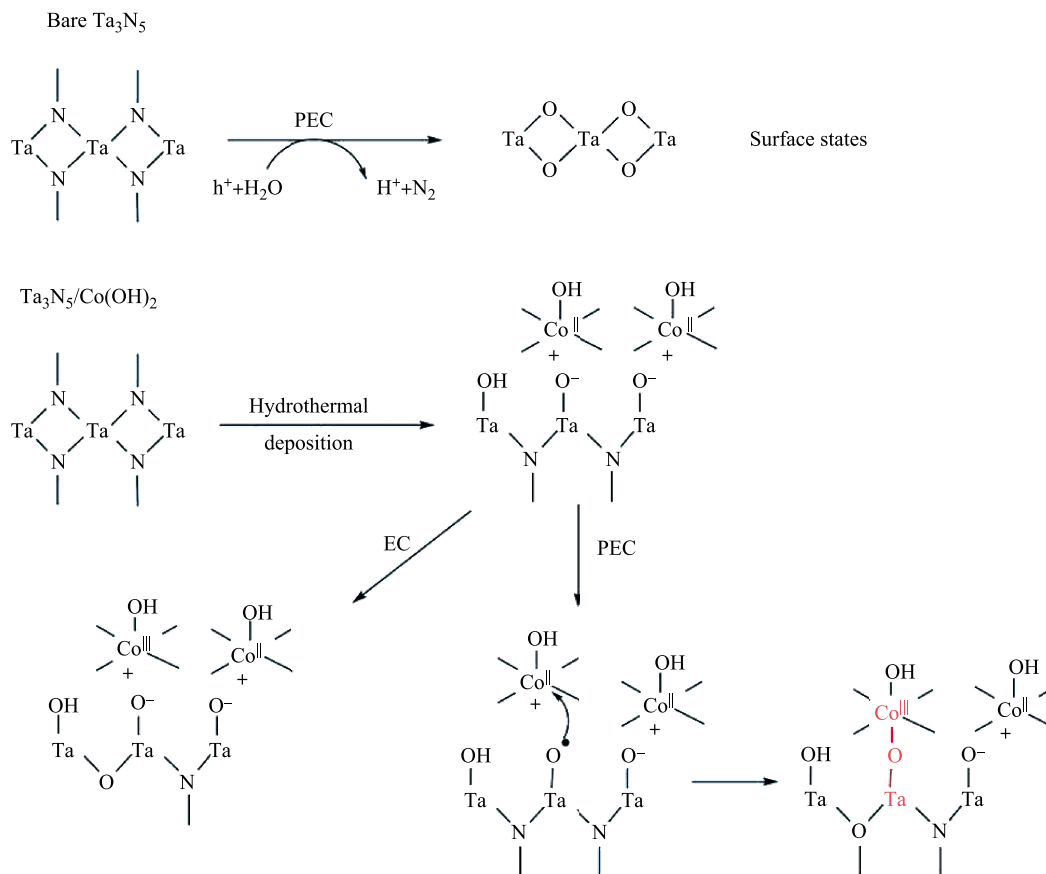


Fig. 13 Proposed mechanism for the Formation of the Ta-O-Co Bond under PEC Conditions. The surface oxidation of bare Ta_3N_5 and the electrochemical oxidation of $\text{Ta}_3\text{N}_5/\text{Co}(\text{OH})_2$ are included for comparison. Reproduced from Refs. [147, 148], Copyright © 2017 Elsevier.

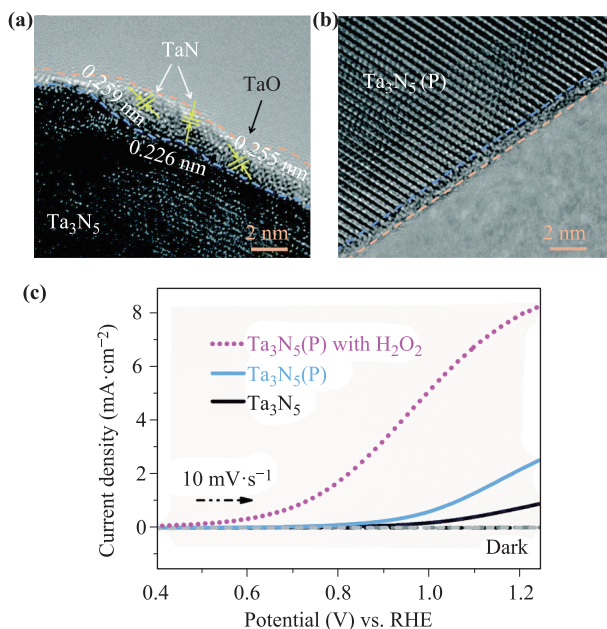


Fig. 14 (a) The HRTEM image of the as-prepared Ta_3N_5 photoanode. (b) HRTEM image of the post treated $\text{Ta}_3\text{N}_5(\text{P})$ photoanode. (c) Current–potential curves of pristine Ta_3N_5 , $\text{Ta}_3\text{N}_5(\text{P})$ photoanodes and the $\text{Ta}_3\text{N}_5(\text{P})$ photoanode with H_2O_2 under AM 1.5G simulated sunlight at $100 \text{ mW}\cdot\text{cm}^{-2}$ in 1 M NaOH aqueous solution (pH = 13.6). Reproduced from Ref. [156], Copyright © 2016 Royal Society of Chemistry.

nificantly improved compared to that of 0.8 V vs. RHE for bare Ta_3N_5 . The onset potential for $\text{CoPi}/\text{Ta}_3\text{N}_5$ is 0.8 V vs. RHE, whereas the onset potential for $\text{CoPi}/\text{GaN}/\text{Ta}_3\text{N}_5$ is 0.65 V, although the VB offset between $\text{GaN}-\text{Ta}_3\text{N}_5$ introduced over-potential. In addition, $\text{CoPi}/\text{GaN}/\text{Ta}_3\text{N}_5$ is stable over 10 h, whereas the photocurrent density of $\text{CoPi}/\text{Ta}_3\text{N}_5$ faded away about in an hour.

A universal method or protocol for passivation layer is highly desired by the community. Recently, the amorphous titanium oxide have drew great attention [165]. Such a layer prepared by atomic layer deposition (ALD) is still conductive enough with the thickness over 100 nm. It serves as both passivation layer and hole transports layer to prevent the photoanode contact with electrolyte directly, which could transfer hole effectively. It was used widely with various photoanodes, such as BiVO_4 [166], Ta_3N_5 [156], Si-based SC [167–169], and GaAs [165]. Such a universal passivation layer can be prepared by electrodeposition as well, which lowered the requirement of instruments [166]. A passivated W-doped BiVO_4 by this manner showed an onset potential shift of -500 mV and were stable over 12 h. In addition, Liu *et al.* [156] have reported that coating of amorphous titanium oxide on Ta_3N_5 surface by a chemical bath of TiCl_3 solution followed by mild curing step. The TiO_x layer significantly enhanced charge injection efficiency and the photocurrent increased from 6.8 to $10.7 \text{ mA}/\text{cm}^2$. It was also shown to serve as electron blocking layer that separates back electron and sur-

face stored holes in the hole-storage layer, and suppresses the electron–hole pairs recombination at surface.

5 Outlook

In PEC systems, the more complicated nature of OER reaction determined that the water oxidation process on photoanodes is usually the rate limiting step for the whole circuit. The high efficiency unbiased water oxidation with visible light, which containing more than 40% of solar energy, is one of the holy grails of this field. Such an ultimate goal raised several requirements for the development of photoanodic materials. In this review, we briefly discussed how these issues were addressed from the consideration of crystal defects, which is a different angle of view in comparison of perfect materials. The imperfectness provides unique interactions in the SC, on the SC and the SC-solution or SC-substrate interface, with optical, electronic and chemical impacts of both pros and cons.

Considering the complexity of chemistry in the preparation, it is usually very challenging to only produce desired defects. Furthermore, even only with a certain type of defect, it may act as a double edge sword, for instance, introducing additional carrier but also serving as scattering or recombination centers. Therefore, the preparation of efficient photoanode highly relies on the optimization on experimental conditions. The understanding of speciation of defects and their role may not be able to precisely predict the behavior of a new material but can provide important guiding information that greatly shorten the period for optimizations. Necessary characterizations which provide these key understandings include those focusing on the structural aspects such as composition, lattice parameters, microstructures, and the spectroscopic features reflecting the electronic nature of the materials. These measurements bridge the gap between synthesis conditions and the performance, so that at least the general trend of the optimization in synthesis can be specified and save considerable amounts of workloads.

Compared with bulk defects, working with the surface defects or surface states is a more complicated issue. The complication comes from two aspects. First, the surface defect is dynamically interacting with the environment. Such a scenario means the species and structures need to be characterized and considered with its operando condition, or at least a double check of spent photoanodes. Second, the surface defects are even more sensitive to the preparation aspects, for instance, the same nano-/microstructure with different crystal facets could have very different surface chemistry behaviors. Given the complexity of exposing SC surface to the electrolyte solution, a completely covered passivation layer is a much easier route for designing new photoanodes. However, the limitation still exists because such a uniform high-quality coating is not easy to prepare particularly for three-dimensional

nanostructured SC electrodes. On the other hand, considering the cost-effectiveness as a key limiting factor for future practical application, such a coating/deposition should be with low cost. Currently, most of the photoanodes with champion performances were prepared using advanced deposition methods, i.e., ALD, PLD and sputtering. Development of simple and scalable functional coating with either cocatalyst or passivation layer are desired.

In short, the presence of defects is a double-edged sword to the SC photoanode for solar water splitting. In the development process, a motif emphasizing the profound connection need to be always carefully considered. The logic chain includes the preparation conditions, the material structure, the subsequent properties, and finally, the photoelectrode performance. Both synthesis methods and characterizations are important to the control of defects. Even great efforts have been made on controlling the defects, many details are still likely to remain unclear particularly for emerging new ternary oxides and new interfaces. In this context, in-situ characterization methods will become more and more important to understand both the formation and the evolution of defects during the synthesis and in operando conditions. Studies to the preparation works are differentiating into two types, either using advanced techniques to break the records, or developing scalable procedures with competitive state-of-the-art performance.

Acknowledgements We thank the editor for the kind invitation. We acknowledge the financial support by the National Natural Science Foundation of China (NSFC, Grant No. 21805298) and Ningbo 3315 Program.

References

- Z. Wang, Y. Inoue, T. Hisatomi, R. Ishikawa, Q. Wang, T. Takata, S. S. Chen, N. Shibata, Y. Ikuhara, and K. Domen, Overall water splitting by Ta₃N₅ nanorod single crystals grown on the edges of KTaO₃ particles, *Nat. Catal.* 1(10), 756 (2018)
- J. Ran, J. Zhang, J. Yu, M. Jaroniec, and S. Z. Qiao, Earth-abundant cocatalysts for semiconductor-based photocatalytic water splitting, *Chem. Soc. Rev.* 43(22), 7787 (2014)
- T. Hisatomi, J. Kubota, and K. Domen, Recent advances in semiconductors for photocatalytic and photoelectrochemical water splitting, *Chem. Soc. Rev.* 43(22), 7520 (2014)
- M. G. Walter, E. L. Warren, J. R. McKone, S. W. Boettcher, Q. Mi, E. A. Santori, and N. S. Lewis, Solar water splitting cells, *Chem. Rev.* 110(11), 6446 (2010)
- Y. Kuang, Q. Jia, G. Ma, T. Hisatomi, T. Minegishi, H. Nishiyama, M. Nakabayashi, N. Shibata, T. Yamada, A. Kudo, and K. Domen, Ultrastable low-bias water splitting photoanodes via photocorrosion inhibition and in situ catalyst regeneration, *Nat. Energy* 2(1), 16191 (2017)
- N. S. Lewis, Research opportunities to advance solar energy utilization, *Science* 351(6271), aad1920 (2016)
- S. Chen and L. W. Wang, Thermodynamic oxidation and reduction potentials of photocatalytic semiconductors in aqueous solution, *Chem. Mater.* 24(18), 3659 (2012)
- J. Y. Kim, G. Magesh, D. H. Youn, J. W. Jang, J. Kubota, K. Domen, and J. S. Lee, Single-crystalline, wormlike hematite photoanodes for efficient solar water splitting, *Sci. Rep.* 3(1), 2681 (2013)
- J. Seo, M. Nakabayashi, T. Hisatomi, N. Shibata, T. Minegishi, M. Katayama, and K. Domen, The effects of annealing barium niobium oxynitride in argon on photoelectrochemical water oxidation activity, *J. Mater. Chem. A Mater. Energy Sustain.* 7(2), 493 (2019)
- T. W. Kim and K. S. Choi, Nanoporous BiVO₄ photoanodes with dual-layer oxygen evolution catalysts for solar water splitting, *Science* 343(6174), 990 (2014)
- Y. Kuang, Q. Jia, H. Nishiyama, T. Yamada, A. Kudo, and K. Domen, A front-illuminated nanostructured transparent BiVO₄ photoanode for >2% efficient water splitting, *Adv. Energy Mater.* 6(2), 1501645 (2016)
- J. Yang, J. K. Cooper, F. M. Toma, K. A. Walczak, M. Favaro, J. W. Beeman, L. H. Hess, C. Wang, C. Zhu, S. Gul, J. Yano, C. Kisielowski, A. Schwartzberg, and I. D. Sharp, A multifunctional biphasic water splitting catalyst tailored for integration with high-performance semiconductor photoanodes, *Nat. Mater.* 16(3), 335 (2017)
- X. Li, S. Liu, K. Fan, Z. Liu, B. Song, and J. Yu, MOF-based transparent passivation layer modified ZnO nanorod arrays for enhanced photo-electrochemical water splitting, *Adv. Energy Mater.* 8(18), 1800101 (2018)
- K. Sivula and R. van de Krol, Semiconducting materials for photoelectrochemical energy conversion, *Nat. Rev. Mater.* 1(2), 15010 (2016)
- J. Nowotny, M. A. Alim, T. Bak, M. A. Idris, M. Ionescu, K. Prince, M. Z. Sahdan, K. Sopian, M. A. Mat Teridi, and W. Sigmund, Defect chemistry and defect engineering of TiO₂-based semiconductors for solar energy conversion, *Chem. Soc. Rev.* 44(23), 8424 (2015)
- S. Sato, R. Nakane, T. Hada, and M. Tanaka, Spin injection into silicon in three-terminal vertical and four-terminal lateral devices with Fe/Mg/MgO/Si tunnel junctions having an ultrathin Mg insertion layer, *Phys. Rev. B* 96(23), 235204 (2017)
- N. S. J. Frougier, D. Deng, M. Jerry, A. Aziz, L. Liu, G. Lavallee, T. S. Mayer, S. Gupta, and S. Datta, Phase-transition-FET exhibiting steep switching slope of 8 mV/decade and 36% enhanced ON current, *IEEE Symposium on VLSI Technology* 2158 (2016)
- W. Zhang, D. Yan, X. Tong, and M. Liu, Ultrathin lutetium oxide film as an epitaxial hole-blocking layer for crystalline bismuth vanadate water splitting photoanodes, *Adv. Funct. Mater.* 28(10), 1705512 (2018)
- F. L. Souza, K. P. Lopes, E. Longo, and E. R. Leite, The influence of the film thickness of nanostructured alpha-Fe₂O₃ on water photooxidation, *Phys. Chem. Chem. Phys.* 11(8), 1215 (2009)

20. O. Zandi, B. M. Klahr, and T. W. Hamann, Highly photoactive Ti-doped α -Fe₂O₃ thin film electrodes: Resurrection of the dead layer, *Energy Environ. Sci.* 6(2), 634 (2013)
21. F. Le Formal, S. R. Pendlebury, M. Cornuz, S. D. Tilley, M. Grätzel, and J. R. Durrant, Back electron-hole recombination in hematite photoanodes for water splitting, *J. Am. Chem. Soc.* 136(6), 2564 (2014)
22. W. Zhang, D. Yan, K. Appavoo, J. Cen, Q. Wu, A. Orlov, M. Y. Sfeir, and M. Liu, Unravelling photocarrier dynamics beyond the space charge region for photoelectrochemical water splitting, *Chem. Mater.* 29(9), 4036 (2017)
23. M. Huang, C. Li, L. Zhang, Q. Chen, Z. Zhen, Z. Li, and H. Zhu, Twin structure in BiVO₄ photoanodes boosting water oxidation performance through enhanced charge separation and transport, *Adv. Energy Mater.* 8(32), 1802198 (2018)
24. Y. Liang, T. Tsubota, L. P. A. Mooij, and R. van de Krol, Highly improved quantum efficiencies for thin film BiVO₄ photoanodes, *J. Phys. Chem. C* 115(35), 17594 (2011)
25. S. Byun, B. Kim, S. Jeon, and B. Shin, Effects of a SnO₂ hole blocking layer in a BiVO₄-based photoanode on photoelectrocatalytic water oxidation, *J. Mater. Chem. A Mater. Energy Sustain.* 5(15), 6905 (2017)
26. Y. Asakura, T. Higashi, H. Nishiyama, H. Kobayashi, M. Nakabayashi, N. Shibata, T. Minegishi, T. Hisatomi, M. Katayama, T. Yamada, and K. Domen, Activation of a particulate Ta₃N₅ water-oxidation photoanode with a GaN hole-blocking layer, *Sustainable Energy Fuels* 2(1), 73 (2018)
27. E. Alarcón-Lladó, L. Chen, M. Hettick, N. Mashouf, Y. Lin, A. Javey, and J. W. Ager, BiVO₄ thin film photoanodes grown by chemical vapor deposition, *Phys. Chem. Chem. Phys.* 2014(4), 1651 (2014)
28. A. Annamalai, P. S. Shinde, A. Subramanian, J. Y. Kim, J. H. Kim, S. H. Choi, J. S. Lee, and J. S. Jang, Bi-functional TiO₂ underlayer for α -Fe₂O₃ nanorod based photoelectrochemical cells: Enhanced interface and Ti⁴⁺ doping, *J. Mater. Chem. A Mater. Energy Sustain.* 3(9), 5007 (2015)
29. T. Hisatomi, H. Dotan, M. Stefik, K. Sivula, A. Rothschild, M. Gratzel, and N. Mathews, Enhancement in the performance of ultrathin hematite photoanode for water splitting by an oxide underlayer, *Adv. Mater.* 24(20), 2699 (2012)
30. Y. Pihosh, I. Turkevych, K. Mawatari, T. Asai, T. Hisatomi, J. Uemura, M. Tosa, K. Shimamura, J. Kubota, K. Domen, and T. Kitamori, Nanostructured WO₃/BiVO₄ photoanodes for efficient photoelectrochemical water splitting, *Small* 10(18), 3692 (2014)
31. X. Shi, I. Y. Choi, K. Zhang, J. Kwon, D. Y. Kim, J. K. Lee, S. H. Oh, J. K. Kim, and J. H. Park, Efficient photoelectrochemical hydrogen production from bismuth vanadate-decorated tungsten trioxide helix nanostructures, *Nat. Commun.* 5(1), 4775 (2014)
32. A. Hayakawa, O. Yoshikawa, T. Fujieda, K. Uehara, and S. Yoshikawa, High performance polythiophene/fullerene bulk-heterojunction solar cell with a TiO_x hole blocking layer, *Appl. Phys. Lett.* 90(16), 163517 (2007)
33. W. Ke, G. Fang, J. Wan, H. Tao, Q. Liu, L. Xiong, P. Qin, J. Wang, H. Lei, G. Yang, M. Qin, X. Zhao, and Y. Yan, Efficient hole-blocking layer-free planar halide perovskite thin-film solar cells, *Nat. Commun.* 6(1), 6700 (2015)
34. P. Chakthranont, T. R. Hellstern, J. M. McEnaney, and T. F. Jaramillo, Design and fabrication of a precious metal-free tandem core-shell p+n Si/W-doped BiVO₄ photoanode for unassisted water splitting, *Adv. Energy Mater.* 7(22), 1701515 (2017)
35. T. Hisatomi, J. Brillet, M. Cornuz, F. Le Formal, N. Tétreault, K. Sivula, and M. Grätzel, A Ga₂O₃ underlayer as an isomorphic template for ultrathin hematite films toward efficient photoelectrochemical water splitting, *Faraday Discuss.* 155, 223 (2012)
36. P. M. Rao, L. Cai, C. Liu, I. S. Cho, C. H. Lee, J. M. Weisse, P. Yang, and X. Zheng, Simultaneously efficient light absorption and charge separation in WO₃/BiVO₄ core/shell nanowire photoanode for photoelectrochemical water oxidation, *Nano Lett.* 14(2), 1099 (2014)
37. B. Lamm, L. Zhou, P. Rao, and M. Stefik, Atomic layer deposition of space-efficient SnO₂ underlayers for BiVO₄ host-guest architectures for photoassisted water splitting, *ChemSusChem* 12, 1 (2018)
38. H. Fujishima and K. Honda, Electrochemical photolysis of water at a semiconductor electrode, *Nature* 238(5358), 37 (1972)
39. T. Ohno, T. Mitsui, and M. Matsumura, Photocatalytic activity of S-doped TiO₂ photocatalyst under visible light, *Chem. Lett.* 32(4), 364 (2003)
40. N. Liu, V. Haublein, X. Zhou, U. Venkatesan, M. Hartmann, M. Mackovic, T. Nakajima, E. Spiecker, A. Osvet, L. Frey, and P. Schmuki, "Black" TiO₂ nanotubes formed by high-energy proton implantation show noble-metal-co-catalyst free photocatalytic H₂-evolution, *Nano Lett.* 15(10), 6815 (2015)
41. X. Chen, L. Liu, P. Y. Yu, and S. S. Mao, Increasing solar absorption for photocatalysis with black hydrogenated titanium dioxide nanocrystals, *Science* 331(6018), 746 (2011)
42. J. Cai, M. Wu, Y. Wang, H. Zhang, M. Meng, Y. Tian, X. Li, J. Zhang, L. Zheng, and J. Gong, Synergetic enhancement of light harvesting and charge separation over surface-disorder-engineered TiO₂ photonic crystals, *Chem* 2(6), 877 (2017)
43. Y. Yang, L. C. Yin, Y. Gong, P. Niu, J. Q. Wang, L. Gu, X. Chen, G. Liu, L. Wang, and H. M. Cheng, An unusual strong visible-light absorption band in red anatase TiO₂ photocatalyst induced by atomic hydrogen-occupied oxygen vacancies, *Adv. Mater.* 30(6), 1704479 (2018)
44. R. Asahi, T. Morikawa, and K. A. Ohwaki, Visible-light photocatalysis in nitrogen-doped titanium oxides, *Science* 293(5528), 269 (2001)
45. S. Sakthivel, M. Janczarek, and H. Kisch, Visible light activity and photoelectrochemical properties of nitrogen-doped TiO₂, *J. Phys. Chem. B* 108(50), 19384 (2004)

46. X. Wang, R. Long, D. Liu, D. Yang, C. Wang, and Y. Xiong, Enhanced full-spectrum water splitting by confining plasmonic Au nanoparticles in N-doped TiO₂ bowl nanoarrays, *Nano Energy* 24, 87 (2016)
47. T. M. R. Asahi, T. Ohwaki, and K. Aoki, Visible-light photocatalysis in nitrogen-doped titanium oxides, *Science* 293(5528), 269 (2001)
48. G. Wang, X. Xiao, W. Li, Z. Lin, Z. Zhao, C. Chen, C. Wang, Y. Li, X. Huang, L. Miao, C. Jiang, Y. Huang, and X. Duan, Significantly enhanced visible light photoelectrochemical activity in TiO₂ nanowire arrays by nitrogen implantation, *Nano Lett.* 15(7), 4692 (2015)
49. T. Lin, C. Yang, Z. Wang, H. Yin, X. Lü, F. Huang, J. Lin, X. Xie, and M. Jiang, Effective nonmetal incorporation in black titania with enhanced solar energy utilization, *Energy Environ. Sci.* 7(3), 967 (2014)
50. S. Hejazi, N. T. Nguyen, A. Mazare, and P. Schmuki, Aminated TiO₂ nanotubes as a photoelectrochemical water splitting photoanode, *Catal. Today* 281, 189 (2017)
51. S. A. Ansari and M. H. Cho, Highly visible light responsive, narrow band gap TiO₂ nanoparticles modified by elemental red phosphorus for photocatalysis and photoelectrochemical applications, *Sci. Rep.* 6(1), 25405 (2016)
52. S. Komatsuda, Y. Asakura, J. J. M. Vequizo, A. Yamakata, and S. Yin, Enhanced photocatalytic NO decomposition of visible-light responsive F-TiO₂/(N, C)-TiO₂ by charge transfer between F-TiO₂ and (N, C)-TiO₂ through their doping levels, *Appl. Catal. B* 238, 358 (2018)
53. X. Kang, X. Z. Song, Y. Han, J. Cao, and Z. Tan, Defect-engineered TiO₂ hollow spiny nanocubes for phenol degradation under visible light irradiation, *Sci. Rep.* 8(1), 5904 (2018)
54. J. Premkumar, Development of super-hydrophilicity on nitrogen-doped TiO₂ thin film surface by photoelectrochemical method under visible light, *Chem. Mater.* 16(21), 3980 (2004)
55. S. A. Ansari, M. M. Khan, M. O. Ansari, and M. H. Cho, Nitrogen-doped titanium dioxide (N-doped TiO₂) for visible light photocatalysis, *New J. Chem.* 40(4), 3000 (2016)
56. X. Pan, M. Q. Yang, X. Fu, N. Zhang, and Y. J. Xu, Defective TiO₂ with oxygen vacancies: Synthesis, properties and photocatalytic applications, *Nanoscale* 5(9), 3601 (2013)
57. H. Choi, D. Shin, B. C. Yeo, T. Song, S. S. Han, N. Park, and S. Kim, Simultaneously controllable doping sites and the activity of a W–N codoped TiO₂ photocatalyst, *ACS Catal.* 6(5), 2745 (2016)
58. Q. Sun, D. Cortie, S. Zhang, T. J. Frankcombe, G. She, J. Gao, L. R. Sheppard, W. Hu, H. Chen, S. Zhuo, D. Chen, R. L. Withers, G. McIntyre, D. Yu, W. Shi, and Y. Liu, The formation of defect-pairs for highly efficient visible-light catalysts, *Adv. Mater.* 29(11), 1605123 (2017)
59. H. Cui, W. Zhao, C. Yang, H. Yin, T. Lin, Y. Shan, Y. Xie, H. Gu, and F. Huang, Black TiO₂ nanotube arrays for high-efficiency photoelectrochemical water-splitting, *J. Mater. Chem. A Mater. Energy Sustain.* 2(23), 8612 (2014)
60. J. Liang, N. Wang, Q. Zhang, B. Liu, X. Kong, C. Wei, D. Zhang, B. Yan, Y. Zhao, and X. Zhang, Exploring the mechanism of a pure and amorphous black-blue TiO₂:H thin film as a photoanode in water splitting, *Nano Energy* 42, 151 (2017)
61. M. Krzywiecki, L. Grzadziel, A. Sarfraz, D. Iqbal, A. Szwejca, and A. Erbe, Zinc oxide as a defect-dominated material in thin films for photovoltaic applications – Experimental determination of defect levels, quantification of composition, and construction of band diagram, *Phys. Chem. Chem. Phys.* 17(15), 10004 (2015)
62. R. A. Wahyuono, F. Hermann-Westendorf, A. Dellith, C. Schmidt, J. Dellith, J. Plentz, M. Schulz, M. Presselt, M. Seyring, M. Rettenmeyer, and B. Dietzek, Effect of annealing on the sub-bandgap, defects and trapping states of ZnO nanostructures, *Chem. Phys.* 483–484, 112 (2017)
63. Y. Zhang, H. Zhao, X. Zhao, J. Lin, N. Li, Z. Huo, Z. Yan, M. Zhang, and S. Hu, Narrow-bandgap Nb₂O₅ nanowires with enclosed pores as high-performance photocatalyst, *Sci. China Mater.* 62(2), 203 (2019)
64. W. L. M. Lamers, M. Favaro, D. E. Starr, D. Friedrich, S. Lardhi, L. Cavallo, M. Harb, R. van de Krol, L. H. Wong, and F. F. Abdi, Enhanced carrier transport and bandgap reduction in sulfur modified BiVO₄ photoanodes, *Chem. Mater.* 30, 8630 (2018)
65. V. Pasumarthi, T. Liu, M. Dupuis, and C. Li, Charge carrier transport dynamics in W/Mo-doped BiVO₄: First principles-based mesoscale characterization, *J. Mater. Chem. A Mater. Energy Sustain.* 7(7), 3054 (2019)
66. T. Li, J. He, B. Pena, and C. P. Berlinguette, Curing BiVO₄ photoanodes with ultraviolet light enhances photoelectrocatalysis, *Angew. Chem. Int. Ed.* 55(5), 1769 (2016)
67. R. Niishiro, Y. Takano, Q. Jia, M. Yamaguchi, A. Iwase, Y. Kuang, T. Minegishi, T. Yamada, K. Domen, and A. Kudo, A CoO_x-modified SnNb₂O₆ photoelectrode for highly efficient oxygen evolution from water, *Chem. Commun. (Camb.)* 53(3), 629 (2017)
68. Y. Hosogi, Y. Shimodaira, H. Kato, H. Kobayashi, and A. Kudo, Role of Sn²⁺ in the band structure of SnM₂O₆ and Sn₂M₂O₇ (M = Nb and Ta) and their photocatalytic properties, *Chem. Mater.* 20(4), 1299 (2008)
69. Y. Shimodaira, H. Kato, H. Kobayashi, and A. Kudo, Investigations of electronic structures and photocatalytic activities under visible light irradiation of lead molybdate replaced with chromium (VI), *Bull. Chem. Soc. Jpn.* 80(5), 885 (2007)
70. D. Noureldine and K. Takanabe, State-of-the-art Sn²⁺-based ternary oxides as photocatalysts for water splitting: Electronic structures and optoelectronic properties, *Catal. Sci. Technol.* 6(21), 7656 (2016)
71. H. Seo, Y. Ping, and G. Galli, Role of point defects in enhancing the conductivity of BiVO₄, *Chem. Mater.* 30(21), 7793 (2018)
72. F. F. Abdi, T. J. Savenije, M. M. May, B. Dam, and R. van de Krol, The origin of slow carrier transport in BiVO₄ thin film photoanodes: A time-resolved microwave conductivity study, *J. Phys. Chem. Lett.* 4(16), 2752 (2013)

73. Z. Zhu, P. Sarker, C. Zhao, L. Zhou, R. L. Grimm, M. N. Huda, and P. M. Rao, Photoelectrochemical properties and behavior of alpha-SnWO₄ photoanodes synthesized by hydrothermal conversion of WO₃ films, *ACS Appl. Mater. Interfaces* 9(2), 1459 (2017)
74. A. Ziani, M. Harb, D. Noureldine, and K. Takanabe, UV-Vis optoelectronic properties of a-SnWO₄: A comparative experimental and density functional theory based study, *APL Mater.* 3(9), 096101 (2015)
75. D. Bohra and W. A. Smith, Improved charge separation via Fe-doping of copper tungstate photoanodes, *Phys. Chem. Chem. Phys.* 17(15), 9857 (2015)
76. Y. Gao and T. W. Hamann, Quantitative hole collection for photoelectrochemical water oxidation with CuWO₄, *Chem. Commun.* 53(7), 1285 (2017)
77. S. Byun, G. Jung, Y. Shi, M. Lanza, and B. Shin, Aging of a vanadium precursor solution: Influencing material properties and photoelectrochemical water oxidation performance of solution-processed BiVO₄ photoanodes, *Adv. Funct. Mater.* 1806662 (2019)
78. M. Ziwrtsch, S. Müller, H. Hempel, T. Unold, F. F. Abdi, R. van de Krol, D. Friedrich, and R. Eichberger, Direct time-resolved observation of carrier trapping and polaron conductivity in BiVO₄, *ACS Energy Lett.* 1(5), 888 (2016)
79. B. J. Trzeźniewski, I. A. Digdaya, T. Nagaki, S. Ravishankar, I. Herraiz-Cardona, D. A. Vermaas, A. Longo, S. Gimenez, and W. A. Smith, Near-complete suppression of surface losses and total internal quantum efficiency in BiVO₄ photoanodes, *Energy Environ. Sci.* 10(6), 1517 (2017)
80. J. K. Cooper, S. B. Scott, Y. Ling, J. Yang, S. Hao, Y. Li, F. M. Toma, M. Stutzmann, K. V. Lakshmi, and I. D. Sharp, Role of hydrogen in defining the n-type character of BiVO₄ photoanodes, *Chem. Mater.* 28(16), 5761 (2016)
81. F. F. Abdi, N. Firet, and R. van de Krol, Efficient BiVO₄ thin film photoanodes modified with cobalt phosphate catalyst and W-doping, *ChemCatChem* 5(2), 490 (2013)
82. Y. Bu, J. Tian, Z. Chen, Q. Zhang, W. Li, F. Tian, and J. P. Ao, Optimization of the photo-electrochemical performance of Mo-Doped BiVO₄ photoanode by controlling the metal-oxygen bond state on (020) facet, *Adv. Mater. Interfaces* 4(10), 1601235 (2017)
83. S. K. Cho, H. S. Park, H. C. Lee, K. M. Nam, and A. J. Bard, Metal doping of BiVO₄ by composite electrodeposition with improved photoelectrochemical water oxidation, *J. Phys. Chem. C* 117(44), 23048 (2013)
84. J. H. Xin Zhao, X. Yao, S. Chen, and Z. Chen, Clarifying the roles of oxygen vacancy in W-doped BiVO₄ for solar water splitting, *ACS Appl. Energy Mater.* 1(7), 3410 (2018)
85. V. Nair, C. L. Perkins, Q. Lin, and M. Law, Textured nanoporous Mo:BiVO₄ photoanodes with high charge transport and charge transfer quantum efficiencies for oxygen evolution, *Energy Environ. Sci.* 9(4), 1412 (2016)
86. G. V. Govindaraju, J. M. Morbec, G. A. Galli, and K. S. Choi, Experimental and computational investigation of lanthanide ion doping on BiVO₄ photoanodes for solar water splitting, *J. Phys. Chem. C* 122(34), 19416 (2018)
87. K. P. Parmar, H. J. Kang, A. Bist, P. Dua, J. S. Jang, and J. S. Lee, Photocatalytic and photoelectrochemical water oxidation over metal-doped monoclinic BiVO₄ photoanodes, *ChemSusChem* 5(10), 1926 (2012)
88. K. Ding, B. Chen, Z. Fang, Y. Zhang, and Z. Chen, Why the photocatalytic activity of Mo-doped BiVO₄ is enhanced: a comprehensive density functional study, *Phys. Chem. Chem. Phys.* 16(26), 13465 (2014)
89. H. W. Jeong, T. H. Jeon, J. S. Jang, W. Choi, and H. Park, Strategic modification of BiVO₄ for improving photoelectrochemical water oxidation performance, *J. Phys. Chem. C* 117(18), 9104 (2013)
90. J. A. Seabold, K. Zhu, and N. R. Neale, Efficient solar photoelectrolysis by nanoporous Mo:BiVO₄ through controlled electron transport, *Phys. Chem. Chem. Phys.* 16(3), 1121 (2014)
91. H. S. Park, K. E. Kweon, H. Ye, E. Paek, G. S. Hwang, and A. J. Bard, Factors in the metal doping of BiVO₄ for improved photoelectrocatalytic activity as studied by scanning electrochemical microscopy and first-principles density-functional calculation, *J. Phys. Chem. C* 115(36), 17870 (2011)
92. I. Cesar, K. Sivula, A. Kay, R. Zboril, and M. Grätzel, Influence of feature size, film thickness, and silicon doping on the performance of nanostructured hematite photoanodes for solar water splitting, *J. Phys. Chem. C* 113(2), 772 (2009)
93. F. F. Abdi, L. Han, A. H. Smets, M. Zeman, B. Dam, and R. van de Krol, Efficient solar water splitting by enhanced charge separation in a bismuth vanadate-silicon tandem photoelectrode, *Nat. Commun.* 4(1), 2195 (2013)
94. A. J. Rettie, H. C. Lee, L. G. Marshall, J. F. Lin, C. Capan, J. Lindemuth, J. S. McCloy, J. Zhou, A. J. Bard, and C. B. Mullins, Combined charge carrier transport and photoelectrochemical characterization of BiVO₄ single crystals: Intrinsic behavior of a complex metal oxide, *J. Am. Chem. Soc.* 135(30), 11389 (2013)
95. W. Zhang, F. Wu, J. Li, D. Yan, J. Tao, Y. Ping, and M. Liu, Unconventional relation between charge transport and photocurrent via boosting small polaron hopping for photoelectrochemical water splitting, *ACS Energy Lett.* 3(9), 2232 (2018)
96. L. Zhang, X. Ye, M. Boloor, A. Poletayev, N. A. Melosh, and W. C. Chueh, Significantly enhanced photocurrent for water oxidation in monolithic Mo:BiVO₄/SnO₂/Si by thermally increasing the minority carrier diffusion length, *Energy Environ. Sci.* 9(6), 2044 (2016)
97. J. W. Jang, D. Friedrich, S. Müller, M. Lamers, H. Hempel, S. Lardhi, Z. Cao, M. Harb, L. Cavallo, R. Heller, R. Eichberger, R. van de Krol, and F. F. Abdi, Enhancing charge carrier lifetime in metal oxide photoelectrodes through mild hydrogen treatment, *Adv. Energy Mater.* 7(22), 1701536 (2017)
98. D. K. Lee, D. Lee, M. A. Lumley, and K. S. Choi, Progress on ternary oxide-based photoanodes for use in photoelectrochemical cells for solar water splitting, *Chem. Soc. Rev.* 48(7), 2126 (2019)

99. G. Wang, H. Wang, Y. Ling, Y. Tang, X. Yang, R. C. Fitzmorris, C. Wang, J. Z. Zhang, and Y. Li, Hydrogen-treated TiO₂ nanowire arrays for photoelectrochemical water splitting, *Nano Lett.* 11(7), 3026 (2011)
100. N. Guijarro, P. Borno, M. Prévot, X. Yu, X. Zhu, M. Johnson, X. Jeanbourquin, F. Le Formal, and K. Sivula, Evaluating spinel ferrites MFe₂O₄ (M = Cu, Mg, Zn) as photoanodes for solar water oxidation: Prospects and limitations, *Sustainable Energy Fuels* 2(1), 103 (2018)
101. Y. Tang, N. Rong, F. Liu, M. Chu, H. Dong, Y. Zhang, and P. Xiao, Enhancement of the photoelectrochemical performance of CuWO₄ films for water splitting by hydrogen treatment, *Appl. Surf. Sci.* 361, 133 (2016)
102. Y. Ling, G. Wang, J. Reddy, C. Wang, J. Z. Zhang, and Y. Li, The influence of oxygen content on the thermal activation of hematite nanowires, *Angew. Chem. Int. Ed.* 51(17), 4074 (2012)
103. A. Milbrat, W. J. C. Visselaar, Y. Guo, B. Mei, J. Huskens, and G. Mul, Integration of molybdenum-doped, hydrogen-annealed BiVO₄ with silicon microwires for photoelectrochemical applications, *ACS Sustain. Chem. & Eng.* 7(5), 5034 (2019)
104. Y. Zhang, X. Zhang, D. Wang, F. Wan, and Y. Liu, Protecting hydrogenation-generated oxygen vacancies in BiVO₄ photoanode for enhanced water oxidation with conformal ultrathin amorphous TiO₂ layer, *Appl. Surf. Sci.* 403, 389 (2017)
105. G. Wang, Y. Ling, H. Wang, X. Yang, C. Wang, J. Z. Zhang, and Y. Li, Hydrogen-treated WO₃ nanoflakes show enhanced photostability, *Energy Environ. Sci.* 5(3), 6180 (2012)
106. W. Li, P. Da, Y. Zhang, Y. Wang, X. Lin, X. Gong, and G. Zheng, WO₃ nanoflakes for enhanced photoelectrochemical conversion, *ACS Nano* 8(11), 11770 (2014)
107. D. Ma, J. Xie, J. Li, S. Liu, F. Wang, H. Zhang, W. Wang, A. Wang, and H. Sun, Synthesis and hydrogen reduction of nano-sized copper tungstate powders produced by a hydrothermal method, *Int. J. Refract. Met. Hard Mater.* 46, 152 (2014)
108. D. Hu, P. Diao, D. Xu, M. Xia, Y. Gu, Q. Wu, C. Li, and S. Yang, Copper(II) tungstate nanoflake array films: Sacrificial template synthesis, hydrogen treatment, and their application as photoanodes in solar water splitting, *Nanoscale* 8(11), 5892 (2016)
109. J. H. Kim, Y. J. Jang, J. H. Kim, J. W. Jang, S. H. Choi, and J. S. Lee, Defective ZnFe₂O₄ nanorods with oxygen vacancy for photoelectrochemical water splitting, *Nanoscale* 7(45), 19144 (2015)
110. S. Wang, P. Chen, J. H. Yun, Y. Hu, and L. Wang, An electrochemically treated BiVO₄ photoanode for efficient photoelectrochemical water splitting, *Angew. Chem. Int. Ed.* 56(29), 8500 (2017)
111. S. K. Pilli, T. E. Furtak, L. D. Brown, T. G. Deutsch, J. A. Turner, and A. M. Herring, Cobalt-phosphate (Co-Pi) catalyst modified Mo-doped BiVO₄ photoelectrodes for solar water oxidation, *Energy Environ. Sci.* 4(12), 5028 (2011)
112. Q. Shi, S. Murcia-López, P. Tang, C. Flox, J. R. Morante, Z. Bian, H. Wang, and T. Andreu, Role of tungsten doping on the surface states in BiVO₄ photoanodes for water oxidation: Tuning the electron trapping process, *ACS Catal.* 8(4), 3331 (2018)
113. W. Luo, Z. Yang, Z. Li, J. Zhang, J. Liu, Z. Zhao, Z. Wang, S. Yan, T. Yu, and Z. Zou, Solar hydrogen generation from seawater with a modified BiVO₄ photoanode, *Energy Environ. Sci.* 4(10), 4046 (2011)
114. L. Gao, Y. Li, J. Ren, S. Wang, R. Wang, G. Fu, and Y. Hu, Passivation of defect states in anatase TiO₂ hollow spheres with Mg doping: Realizing efficient photocatalytic overall water splitting, *Appl. Catal. B* 202, 127 (2017)
115. C. Chen, Y. Wei, G. Yuan, Q. Liu, R. Lu, X. Huang, Y. Cao, and P. Zhu, Synergistic effect of Si doping and heat treatments enhances the photoelectrochemical water oxidation performance of TiO₂ nanorod arrays, *Adv. Funct. Mater.* 27(31), 1701575 (2017)
116. A. G. Hufnagel, H. Hajiyani, S. Zhang, T. Li, O. Kasian, B. Gault, B. Breitbach, T. Bein, D. Fattakhova-Rohlfing, C. Scheu, and R. Pentcheva, Why tin-doping enhances the efficiency of hematite photoanodes for water splitting—the full picture, *Adv. Funct. Mater.* 28(52), 1804472 (2018)
117. Y. Guo, N. Zhang, X. Wang, Q. Qian, S. Zhang, Z. Li, and Z. Zou, A facile spray pyrolysis method to prepare Ti-doped ZnFe₂O₄ for boosting photoelectrochemical water splitting, *J. Mater. Chem. A Mater. Energy Sustain.* 5(16), 7571 (2017)
118. J. H. Kim, J. H. Kim, J.W. Jang, J. Y. Kim, S. H. Choi, G. Magesh, J. Lee, and J. S. Lee, Awakening solar water-splitting activity of ZnFe₂O₄ nanorods by hybrid microwave annealing, *Adv. Energy Mater.* 5(6), 1401933 (2015)
119. C. D. Morton, I. J. Slipper, M. J. K. Thomas, and B. D. Alexander, Synthesis and characterisation of Fe–V–O thin film photoanodes, *J. Photochem. Photobiol. Chem.* 216(2–3), 209 (2010)
120. G. Peng, J. Albero, H. Garcia, and M. Shalom, A water-splitting carbon nitride photoelectrochemical cell with efficient charge separation and remarkably low onset potential, *Angew. Chem. Int. Ed.* 57(48), 15807 (2018)
121. X. Shi, K. Zhang, K. Shin, J. H. Moon, T. W. Lee, and J. H. Park, Constructing inverse opal structured hematite photoanodes via electrochemical process and their application to photoelectrochemical water splitting, *Phys. Chem. Chem. Phys.* 15(28), 11717 (2013)
122. L. Pei, B. Lv, S. Wang, Z. Yu, S. Yan, R. Abe, and Z. Zou, Oriented growth of Sc-doped Ta₃N₅ nanorod photoanode achieving low-onset-potential for photoelectrochemical water oxidation, *ACS Appl. Energy Mater.* 1(8), 4150 (2018)
123. J. Seo, H. Nishiyama, T. Yamada, and K. Domen, Visible-light-responsive photoanodes for highly active, stable water oxidation, *Angew. Chem. Int. Ed.* 57(28), 8396 (2018)

124. M. Zhong, T. Hisatomi, Y. Kuang, J. Zhao, M. Liu, A. Iwase, Q. Jia, H. Nishiyama, T. Minegishi, M. Nakabayashi, N. Shibata, R. Niishiro, C. Katayama, H. Shibano, M. Katayama, A. Kudo, T. Yamada, and K. Domen, Surface modification of CoO_x loaded BiVO_4 photoanodes with ultrathin p-type NiO layers for improved solar water oxidation, *J. Am. Chem. Soc.* 137(15), 5053 (2015)
125. Z. Zhu, H. Tian, M. Zhang, B. Liang, and W. Li, Preparation of $\alpha\text{-SnWO}_4$ hierarchical spheres by Bi^{3+} -doping and their enhanced photocatalytic activity under visible light, *Ceram. Int.* 42(13), 14743 (2016)
126. S. Yao, M. Zhang, J. Di, Z. Wang, Y. Long, and W. Li, Preparation of $\alpha\text{-SnWO}_4/\text{SnO}_2$ heterostructure with enhanced visible-light-driven photocatalytic activity, *Appl. Surf. Sci.* 357, 1528 (2015)
127. I. S. Cho, C. H. Kwak, D. W. Kim, S. Lee, and K. S. Hong, Photophysical, photoelectrochemical, and photocatalytic properties of novel SnWO_4 oxide semiconductors with narrow band gaps, *J. Phys. Chem. C* 113(24), 10647 (2009)
128. Y. Wang, H. Sun, S. Tan, H. Feng, Z. Cheng, J. Zhao, A. Zhao, B. Wang, Y. Luo, J. Yang, and J. G. Hou, Role of point defects on the reactivity of reconstructed anatase titanium dioxide (001) surface, *Nat. Commun.* 4(1), 2214 (2013)
129. G. Liu, H. G. Yang, X. Wang, L. Cheng, H. Lu, L. Wang, G. Q. M. Lu, and H. M. Cheng, Enhanced photoactivity of oxygen-deficient anatase TiO_2 sheets with dominant {001} facets, *J. Phys. Chem. C* 113(52), 21784 (2009)
130. G. Liu, J. Pan, L. Yin, J. T. S. Irvine, F. Li, J. Tan, P. Wormald, and H. M. Cheng, Heteroatom-modulated switching of photocatalytic hydrogen and oxygen evolution preferences of anatase TiO_2 microspheres, *Adv. Funct. Mater.* 22(15), 3233 (2012)
131. J. Hu, X. Zhao, W. Chen, and Z. Chen, Enhanced charge transport and increased active sites on $\alpha\text{-Fe}_2\text{O}_3$ (110) nanorod surface containing oxygen vacancies for improved solar water oxidation performance, *ACS Omega* 3(11), 14973 (2018)
132. C. Fàbrega, D. Monllor-Satoca, S. Ampudia, A. Parra, T. Andreu, and J. R. Morante, Tuning the Fermi level and the kinetics of surface states of TiO_2 nanorods by means of ammonia treatments, *J. Phys. Chem. C* 117(40), 20517 (2013)
133. A. L. Linsebigler, G. Lu, and J. T. Yates, Photocatalysis on TiO_2 surfaces: Principles, mechanisms, and selected results, *Chem. Rev.* 95(3), 735 (1995)
134. A. Yamakata, T. Ishibashi, and H. Onishi, Kinetics of the photocatalytic water-splitting reaction on TiO_2 and Pt/TiO_2 studied by time-resolved infrared absorption spectroscopy, *J. Mol. Catal. Chem.* 199(1–2), 85 (2003)
135. T. Zhang, Y. Liu, J. Liang, and D. Wang, Enhancement of photoelectrochemical and photocathodic protection properties of TiO_2 nanotube arrays by simple surface UV treatment, *Appl. Surf. Sci.* 394, 440 (2017)
136. T. Zhang, S. Cui, B. Yu, Z. Liu, and D. Wang, Surface engineering for an enhanced photoelectrochemical response of TiO_2 nanotube arrays by simple surface air plasma treatment, *Chem. Commun.* 51(95), 16940 (2015)
137. T. L. Villarreal, R. Gómez, M. Neumann-Spallart, N. Alonso-Vante, and P. Salvador, Semiconductor photooxidation of pollutants dissolved in water: A kinetic model for distinguishing between direct and indirect interfacial hole transfer (I): Photoelectrochemical experiments with polycrystalline anatase electrodes under current doubling and absence of recombination, *J. Phys. Chem. B* 108(39), 15172 (2004)
138. A. Kafizas, Y. Ma, E. Pastor, S. R. Pendlebury, C. Mesa, L. Francàs, F. Le Formal, N. Noor, M. Ling, C. Sotelo-Vazquez, C. J. Carmalt, I. P. Parkin, and J. R. Durrant, Water oxidation kinetics of accumulated holes on the surface of a TiO_2 photoanode: A rate law analysis, *ACS Catal.* 7(7), 4896 (2017)
139. S. H. Szczepankiewicz, A. J. Colussi, and M. R. Hoffmann, Infrared spectra of photoinduced species on hydroxylated titania surfaces, *J. Phys. Chem. B* 104(42), 9842 (2000)
140. M. A. Grela, M. E. J. Coronel, and A. J. Colussi, Quantitative spin-trapping studies of weakly illuminated titanium dioxide sols: Implications for the mechanism of photocatalysis, *J. Phys. Chem.* 100(42), 16940 (1996)
141. X. Cheng, Q. Cheng, X. Deng, P. Wang, and H. Liu, A facile and novel strategy to synthesize reduced TiO_2 nanotubes photoelectrode for photoelectrocatalytic degradation of diclofenac, *Chemosphere* 144, 888 (2016)
142. J. Cheng, J. VandeVondele, and M. Sprik, Identifying trapped electronic holes at the aqueous TiO_2 interface, *J. Phys. Chem. C* 118(10), 5437 (2014)
143. Y. Ji, B. Wang, and Y. Luo, GGA+*U* study on the mechanism of photodecomposition of water adsorbed on rutile TiO_2 (110) surface: Free vs. trapped hole, *J. Phys. Chem. C* 118(2), 1027 (2014)
144. T. Hisatomi, F. Le Formal, M. Cornuz, J. Brilllet, N. Tétreault, K. Sivula, and M. Grätzel, Cathodic shift in onset potential of solar oxygen evolution on hematite by 13-group oxide overlayers, *Energy Environ. Sci.* 4(7), 2512 (2011)
145. Z. Hu, Z. Shen, and J. C. Yu, Covalent fixation of surface oxygen atoms on hematite photoanode for enhanced water oxidation, *Chem. Mater.* 28(2), 564 (2016)
146. C. Li, Z. Luo, T. Wang, and J. Gong, Surface, bulk, and interface: Rational design of hematite architecture toward efficient photo-electrochemical water splitting, *Adv. Mater.* 30(30), 1707502 (2018)
147. Y. He, J. E. Thorne, C. H. Wu, P. Ma, C. Du, Q. Dong, J. Guo, and D. Wang, What limits the performance of Ta_3N_5 for solar water splitting? *Chem* 1(4), 640 (2016)
148. Y. He, P. Ma, S. Zhu, M. Liu, Q. Dong, J. Espano, X. Yao, and D. Wang, Photo-induced performance enhancement of tantalum nitride for solar water oxidation, *Joule* 1(4), 831 (2017)

149. E. Nurlaela, Y. Sasaki, M. Nakabayashi, N. Shibata, T. Yamada, and K. Domen, Towards zero bias photoelectrochemical water splitting: onset potential improvement on a Mg:GaN modified-Ta₃N₅ photoanode, *J. Mater. Chem. A Mater. Energy Sustain.* 6(31), 15265 (2018)
150. Y. Kuang, T. Yamada, and K. Domen, Surface and interface engineering for photoelectrochemical water oxidation, *Joule* 1(2), 290 (2017)
151. P. Y. Tang, H. B. Xie, C. Ros, L. J. Han, M. Biset-Peiró, Y. M. He, W. Kramer, A. P. Rodríguez, E. Saucedo, J. R. Galán-Mascarós, T. Andreu, J. R. Morante, and J. Arbiol, Enhanced photoelectrochemical water splitting of hematite multilayer nanowire photoanodes by tuning the surface state via bottom-up interfacial engineering, *Energy Environ. Sci.* 10(10), 2124 (2017)
152. R. d. Krol and M. Grätzel, Photoelectrochemical Hydrogen Production, Springer, New York, 2011, p 321
153. K. J. McDonald and K. S. Choi, Synthesis and photoelectrochemical properties of Fe₂O₃/ZnFe₂O₄ composite photoanodes for use in solar water oxidation, *Chem. Mater.* 23(21), 4863 (2011)
154. B. Klahr, S. Gimenez, F. Fabregat-Santiago, J. Bisquert, and T. W. Hamann, Electrochemical and photoelectrochemical investigation of water oxidation with hematite electrodes, *Energy Environ. Sci.* 5(6), 7626 (2012)
155. X. Yang, C. Du, R. Liu, J. Xie, and D. Wang, Balancing photovoltage generation and charge-transfer enhancement for catalyst-decorated photoelectrochemical water splitting: A case study of the hematite/MnO_x combination, *J. Catal.* 304, 86 (2013)
156. G. Liu, S. Ye, P. Yan, F. Xiong, P. Fu, Z. Wang, Z. Chen, J. Shi, and C. Li, Enabling an integrated tantalum nitride photoanode to approach the theoretical photocurrent limit for solar water splitting, *Energy Environ. Sci.* 9(4), 1327 (2016)
157. F. F. Abdi and R. van de Krol, Nature and light dependence of bulk recombination in Co-Pi-catalyzed BiVO₄ photoanodes, *J. Phys. Chem. C* 116(17), 9398 (2012)
158. B. Klahr, S. Gimenez, F. Fabregat-Santiago, J. Bisquert, and T. W. Hamann, Photoelectrochemical and impedance spectroscopic investigation of water oxidation with “Co-Pi”-coated hematite electrodes, *J. Am. Chem. Soc.* 134(40), 16693 (2012)
159. D. K. Zhong, M. Cornuz, K. Sivula, M. Grätzel, and D. R. Gamelin, Photo-assisted electrodeposition of cobalt-phosphate (Co-Pi) catalyst on hematite photoanodes for solar water oxidation, *Energy Environ. Sci.* 4(5), 1759 (2011)
160. S. D. Tilley, M. Cornuz, K. Sivula, and M. Grätzel, Light-induced water splitting with hematite: Improved nanostructure and iridium oxide catalysis, *Angew. Chem. Int. Ed.* 49(36), 6405 (2010)
161. W. Y. Sohn, J. E. Thorne, Y. Zhang, S. Kuwahara, Q. Shen, D. Wang, and K. Katayama, Charge carrier kinetics in hematite with NiFeO_x coating in aqueous solutions: Dependence on bias voltage, *J. Photochem. Photobiol. Chem.* 353, 344 (2018)
162. X. Yang, R. Liu, C. Du, P. Dai, Z. Zheng, and D. Wang, Improving hematite-based photoelectrochemical water splitting with ultrathin TiO₂ by atomic layer deposition, *ACS Appl. Mater. Interfaces* 6(15), 12005 (2014)
163. R. Liu, Z. Zheng, J. Spurgeon, and X. Yang, Enhanced photoelectrochemical water-splitting performance of semiconductors by surface passivation layers, *Energy Environ. Sci.* 7(8), 2504 (2014)
164. M. Zhong, T. Hisatomi, Y. Sasaki, S. Suzuki, K. Teshima, M. Nakabayashi, N. Shibata, H. Nishiyama, M. Katayama, T. Yamada, and K. Domen, Highly active GaN-stabilized Ta₃N₅ thin-film photoanode for solar water oxidation, *Angew. Chem. Int. Ed.* 56(17), 4739 (2017)
165. S. Hu, M. R. Shaner, J. A. Beardslee, M. Lichterman, B. S. Brunshwig, and N. S. Lewis, Amorphous TiO₂ coatings stabilize Si, GaAs, and GaP photoanodes for efficient water oxidation, *Science* 344(6187), 1005 (2014)
166. D. Eisenberg, H. S. Ahn, and A. J. Bard, Enhanced photoelectrochemical water oxidation on bismuth vanadate by electrodeposition of amorphous titanium dioxide, *J. Am. Chem. Soc.* 136(40), 14011 (2014)
167. A. G. Scheuermann, J. P. Lawrence, K. W. Kemp, T. Ito, A. Walsh, C. E. Chidsey, P. K. Hurley, and P. C. McIntyre, Design principles for maximizing photovoltage in metal-oxide-protected water-splitting photoanodes, *Nat. Mater.* 15(1), 99 (2016)
168. S. Hu, M. H. Richter, M. F. Lichterman, J. Beardslee, T. Mayer, B. S. Brunshwig, and N. S. Lewis, Electrical, photoelectrochemical, and photoelectron spectroscopic investigation of the interfacial transport and energetics of amorphous TiO₂/Si heterojunctions, *J. Phys. Chem. C* 120(6), 3117 (2016)
169. T. Yao, R. Chen, J. Li, J. Han, W. Qin, H. Wang, J. Shi, F. Fan, and C. Li, Manipulating the interfacial energetics of n-type silicon photoanode for efficient water oxidation, *J. Am. Chem. Soc.* 138(41), 13664 (2016)